

Elastic Electron-Proton Scattering Cross Sections Measured by a Coincidence Technique*

M. GOITEIN,† R. J. BUDNITZ,‡ L. CARROLL,§ J. R. CHEN,|| J. R. DUNNING, JR.,** K. HANSON, D. C. IMRIE,†† C. MISTRETTA,‡‡ AND RICHARD WILSON

Department of Physics, Harvard University, Cambridge, Massachusetts 02138

(Received 10 September 1969)

We have measured elastic electron-proton scattering cross sections in the range of four-momentum transfers from $7 F^{-2} [0.27(\text{GeV}/c)^2]$ to $150 F^{-2} [5.84(\text{GeV}/c)^2]$ and at scattered electron angles of between 20° and 34° in the laboratory. The estimated errors in the cross sections range from $\pm 2.1\%$ at the lowest momentum transfer to $\pm 9.6\%$ at the highest. Both the scattered electron and the recoil proton were detected, resulting in an overdetermination of the kinematics. When the constraint of a coincident proton is removed, there is no significant change in the estimated cross sections.

I. INTRODUCTION

HERE we present an experimental contribution to the information on nucleon structure.¹ Elastic electron-proton scattering cross sections have been measured in the range of four-momentum transfers from $7 F^{-2} [0.27(\text{BeV}/c)^2]$ to $150 F^{-2} [5.84(\text{BeV}/c)^2]$. These measurements, in conjunction with data from other experiments covering different angular regions at similar four-momentum transfers, can be used to extract proton form factors. This experiment was performed in conjunction with measurements of quasi-elastic electron-deuteron scattering,² which yield information concerning the neutron form factors.

Knowledge of the incident electron energy and direction and of one further parameter, the scattered electron angle in this experiment, is sufficient to define completely the two-body elastic kinematics. It is usual to impose one further kinematic restraint, knowledge of the scattered electron energy in this experiment, in order to exclude or substantially reduce backgrounds from inelastic events such as those in which one or more pions are produced. This experiment is unique in that one further redundant kinematic parameter was measured—namely, the angle of the recoiling proton. The investigation of whether an apparent change in the measured value of the cross section occurs when the additional constraint is relaxed constitutes a critical check on the measurement. No previous experiment

has had this degree of overdetermination of the kinematics.

In Sec. II we describe the experimental apparatus. Section III is a brief description of the computer system. The data analysis is presented in Sec. IV and the results, together with a comparison with other data, in Sec. V.

A report of preliminary results of this experiment has already been given.³ The cross sections reported

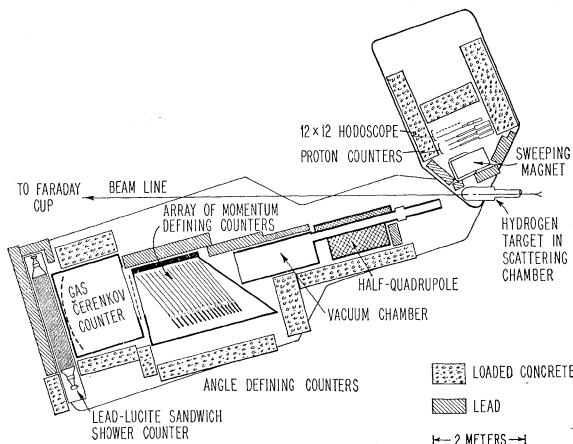


FIG. 1. Plan view of the apparatus (schematic).

here supersede those of Ref. 3, which were the result of a preliminary analysis and were correct within their quoted errors. The present analysis is, however, an improvement on the preliminary one and, in addition, involves some new data not previously presented.

The nominal values of the kinematic variables involved in this experiment are given in Table I. Throughout this paper data are referred to by the value in reciprocal square fermis of the nominal momentum transfer involved.

³ M. Goitein, R. J. Budnitz, L. Carroll, J. Chen, J. R. Dunning, Jr., K. Hanson, D. Imrie, C. Mistretta, J. K. Walker, Richard Wilson, G. F. Dell, M. Fotino, J. M. Paterson, and H. Winick, *Phys. Rev. Letters* **18**, 1016 (1967).

* Work supported by the U.S. Atomic Energy Commission.
 † Partially supported by a Frank Knox Memorial Fellowship and an IBM Fellowship. Present address: Lawrence Radiation Laboratory, Berkeley, Calif.
 ‡ Present address: Lawrence Radiation Laboratory, Berkeley, Calif.
 § Present address: Liverpool University, Liverpool, England.
 || Present address: University of Pennsylvania, Philadelphia, Pa.
 ** Present address: Sonoma State College, Rohnert Park, Calif.
 †† Present address: University College, London, England.
 ‡‡ Present address: University of Wisconsin, Madison, Wisc.
¹ A fuller description of this material is presented in M. Goitein's Ph.D. thesis (unpublished), copies of which are available from the Librarian, Widener Library, Harvard University.
² R. Budnitz, J. Appel, L. Carroll, J. Chen, J. R. Dunning, Jr., M. Goitein, K. Hanson, D. Imrie, C. Mistretta, J. K. Walker, and Richard Wilson, *Phys. Rev. Letters* **19**, 809 (1967); *Phys. Rev.* **173**, 1357 (1968).

TABLE I. List of the kinematic variables involved in the present experiment. The italicized entry (either incident electron energy or scattered electron angle), together with the four-momentum transfer, defines the nominal kinematics for a given datum point. Cross sections are corrected from their measured value so as to be relevant to the nominal kinematics. The last two columns indicate the magnified (fractional) effect on the cross section of small (fractional) changes in the incident electron energy and scattered electron angle.

Four-momentum transfer q^2 (F^{-2})	Scattered angle θ (deg)	Electrons Incident energy E_0 (MeV)	Scattered energy E' (MeV)	Angle φ (deg)	Recoil proton Kinetic energy T (MeV)	Momentum P (MeV/c)	Separation between elastic scattering and π production as % of E'	Separation	
								$-\frac{d\sigma}{\sigma}$	$-\frac{d\sigma/\sigma}{dE_0/E_0}$
7.000	20.00	1578	1433	64.69	145.3	542.0	8.9	3.6	5.6
10.00	20.00	1904	1696	61.89	207.6	657.8	7.4	4.1	6.0
15.00	20.00	2362	2051	58.19	311.4	825.4	5.9	4.7	6.5
20.00	20.00	2758	2342	55.22	415.2	975.4	5.1	5.1	7.0
30.00	20.00	3440	2817	50.55	622.8	1248	4.1	5.8	7.5
45.00	20.00	4308	3374	45.41	934.2	1620	3.3	6.4	8.0
70.00	20.16	5500	4047	39.35	1453	2200	2.6	6.9	8.3
75.00	19.06	6000	4443	38.86	1557	2312	2.3	7.1	8.4
90.00	21.68	6000	4132	35.23	1868	2645	2.3	7.1	8.3
100.0	26.29	5500	3424	31.97	2076	2865	2.6	7.1	8.0
115.0	26.28	6000	3613	30.09	2387	3191	2.3	7.2	8.0
130.0	29.29	6000	3301	27.36	2699	3514	2.3	7.1	7.3
150.0	33.77	6000	2886	24.01	3114	3942	2.3	7.0	7.3

II. APPARATUS

A schematic diagram of the apparatus is presented in Fig. 1. The Cambridge Electron Accelerator's external electron beam passed through a liquid-hydrogen target and was stopped some 12 m further downstream in a Faraday cup placed inside a shielding hut. Scattered electrons were detected in a magnetic spectrometer which defined the angular acceptance of the system. Recoil protons were detected by scintillation counters.

A. Incident Electron Beam

The approximate characteristics of the external electron beam are summarized in Table II. The beam position was monitored both by rf cavities and by fluorescent screens viewed by closed-circuit television.

B. Liquid-Hydrogen Cooler and Target

The cryostat was of a well-established design similar to one described in Ref. 4. Cooling was effected by passing cold helium gas through condensing coils in the hydrogen gas. The target cup, liquid reservoir, and gas ballast tank formed a closed system. The pressure drop upon cooling was thus a direct measure of the volume of condensed hydrogen. Moreover, the hydrogen gas pressure measured directly, in the manner of a vapor-pressure thermometer, the temperature and hence density of the liquid. The target cup is depicted in Fig. 2. It was designed to encourage convection rather than boiling as the principal mechanism for heat loss. Visual observation indeed indicated the presence of strong convection currents.

C. Electron Spectrometer

The elements of this spectrometer were (i) half-quadrupole magnet; (ii) defining aperture for the elec-

TABLE II. Characteristics of the CEA external electron beam.

Repetition rate	60 cps
Duty cycle	$\frac{1}{2}$ -3%
Spill duration	300-1200 μ sec
Extraction efficiency	50-70%
Maximum operating intensity	about 2×10^{-7} A
Energy range	0.5 to 6 BeV
Energy spread	$< \pm 1.3\%$ ^a
Stability of peak energy	$\pm 0.05\%$ approximately
Beam profile:	
At target,	
horizontal	3 mm
vertical	1 mm
At Faraday cup	
horizontal	5 cm ^b
vertical	$2\frac{1}{2}$ cm ^b

^a Strongly dependent on spill width.

^b Average values, rather dependent on energy.

⁴ L. Hand, J. Rees, W. Shlaer, J. K. Walker, and Richard Wilson, in *Nucleon Structure*, edited by R. Hofstadter and L. Schiff (Stanford U. P., Stanford, Calif., 1964).

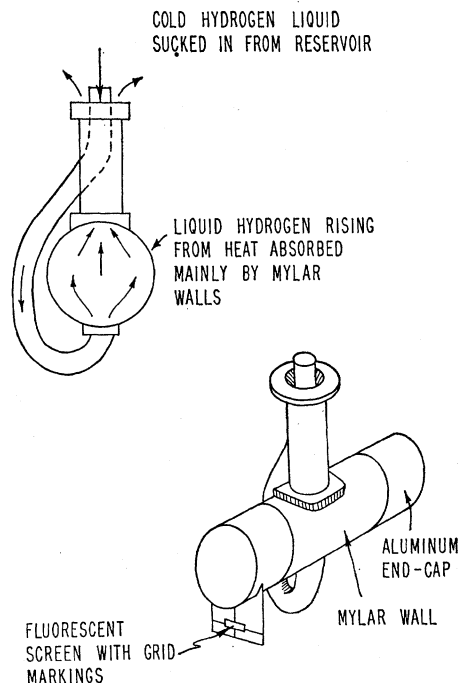


FIG. 2. End and perspective views of the target cup.

tron solid angle; (iii) momentum-defining counters; (iv) threshold gas Čerenkov counter; and (v) lead-Lucite sandwich shower counter. All elements were mounted on a movable platform which pivoted directly below the liquid-hydrogen target. The basic design of single quadrupole spectrometers is well established⁵ and we will mention only briefly the salient features of this one. The momentum defining counter array was the only unusual element. The spectrometer had a total momentum acceptance of 14%, subdivided into bins of about 1% width and a resolution, above 2 BeV/c, of approximately 2% full width at half-maximum (FWHM).

(i) The half quadrupole magnet was a standard C.E.A. 12-in. quadrupole with the iron and coils of one half removed and replaced by a flat iron plate which, acting as a magnetic mirror, preserved the quadrupole nature of the field in the remaining semi-circular aperture. Long flip-coil measurements were made of the field integrating along the length of the magnet. $\int \mathbf{H} \cdot d\mathbf{l}$ was within 1% of that for a full quadrupole of otherwise identical design. A lead "plug" ran the length of the magnet in the horizontal plane.

(ii) Two defining apertures were used during the experiment. The "front aperture" consisted of two tungsten jawed apertures placed just in front of the quadrupole magnet, one above and one below the horizontal plane of the spectrometer. The jaws were angled so as to point at the target and had a small step ma-

⁵ K. W. Chen, J. R. Dunning, Jr., A. A. Cone, N. F. Ramsey, J. K. Walker, and Richard Wilson, *Phys.* **141**, 1267 (1966).

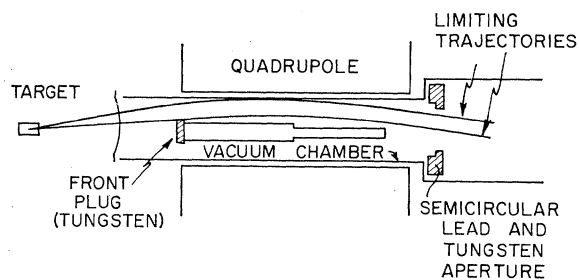


FIG. 3. Rear aperture. Schematic and not to scale.

chined in them to reduce edge uncertainties. The front aperture subtended about 0.83 msr.

The "rear aperture" was defined by several obstacles: A semicircular lead and tungsten aperture behind the quadrupole intercepted in the horizontal direction. A tungsten block in the front of the quadrupole determined the smallest vertical slope permitted and served to divide the aperture into a lower and upper half. Steeply sloping trajectories were delimited by the stainless-steel wall of the vacuum chamber which ran the length of the quadrupole. Figure 3 indicates the location of the various elements of the aperture which subtended 1.8 msr.

(iii) The momentum-defining counters are shown in Fig. 4. Nineteen counters were placed with their top edges in the focusing plane of the quadrupole at 1% momentum intervals (except for four $\frac{1}{2}$ % bins). Six counters were placed above and in contact with certain of the bottom counters and to aid in the pattern-recognition problem, and to simplify triggering. Figure 5 shows a schematic side view of the counter array and a representation of the ideal firing pattern for a falling trajectory—termed an "up-down" trajectory. The counters were made as small as possible in order to reduce singles rates, and consequently a further complication arose, namely, that some counters, such as "+6" in the trajectory depicted in Fig. 5, might not necessarily be involved in the firing pattern which defined a particle-crossing point.

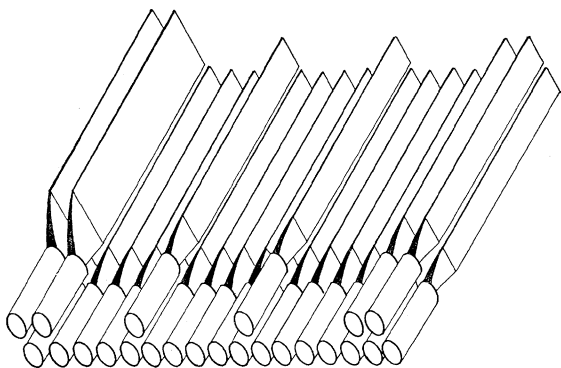


FIG. 4. Perspective view of the momentum defining counters. The target is to the right. Two counters ($-\frac{1}{2}$ % and $+\frac{1}{2}$ %) are not shown.

One advantage of such an array over the conventional configuration which places a series of thin counters in the focal plane of the magnet is that there is no overlap of momentum bins. That is, there is no possibility of two or more adjacent bins being triggered simultaneously by a single trajectory. Another advantage is the detail available for reconstructing an event. In a sense, one has the equivalent of a fast one-dimensional spark chamber. This implies the principal disadvantage, namely, that the pattern recognition procedure is complicated and virtually necessitates the use of a computer.

The counters were pivoted about the quadrupole axis so as to compensate for the kinematic correlation of elastically scattered electron momentum with scattering angle.

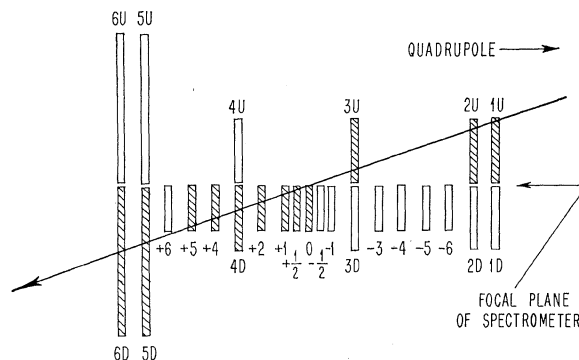


FIG. 5. Typical "up-down" trajectory focusing in 0% bin ("perfect" trajectory). Shaded counters fire, others should not fire (not to scale).

(iv) The threshold gas Čerenkov counter has been described elsewhere.⁶ Filled with Freon C318 gas, the pressure was usually set just below the Čerenkov radiation threshold for pions of the same momentum as the elastically scattered electrons.

(v) The lead-Lucite sandwich shower counter consisted of ten 86×112 cm sheets of UVT Lucite interleaved with ten 1-radiation-length lead sheets and was viewed by eight 5-in. phototubes. Lucite, rather than scintillator, was used in an effort to improve discrimination against pions.⁷ The poor uniformity of light collection almost certainly offset this potential gain and we would recommend the use of scintillator for counters of this size unless extreme care is taken in the light collection. However, we have no detailed information as to the pion rejection which we achieved in practice.

D. Proton Arm

The proton detector consisted of scintillation counters in direct view of the target. They were protected

⁶ A. A. Cone, Ph.D. thesis, Harvard University, 1965 (unpublished); A. A. Cone, K. W. Chen, J. R. Dunning, Jr., G. Hartwig, N. Ramsey, J. K. Walker, and Richard Wilson, *Phys. Rev.* **156**, 1490 (1967).

⁷ C. Heusch and C. Prescott, *Nucl. Instr. Methods* **29**, 125 (1964).

from low-energy charged particles (up to about 40 MeV/c) by a sweeping magnet which provided some 80 kG in. of field.

At the high-momentum transfers (above $70 F^{-2}$), two telescopes were used, each consisting of three scintillation counters. One intercepted all protons associated with electrons elastically scattered out of the target into the upper half of the electron spectrometer acceptance, the other telescope was positioned to receive protons associated with electrons scattered into the lower half of the electron aperture (see Fig. 6).

At $70 F^{-2}$ and below, a single, much larger, telescope of two (sometimes three) scintillation counters was used. It accepted all protons no matter where their associated electrons went in the spectrometer aperture. This telescope was also used in the quasi-elastic electron-deuteron experiment and is described more fully in Ref. 2.

The proton counters were oversized by at least $\frac{1}{2}^\circ$ (subtended at the target) in order to ensure that the system acceptance was determined by the electron aperture alone. This tolerance was sufficient to allow for uncertainties arising from surveying error, beam position changes, energy spread in the incident beam, uncertainty in the effect on protons of the sweeping magnet, and angular upsets involved in scattering accompanied by radiation.

E. Electronic Logic

Signals from all phototubes were fed into discriminators (Chronetics 101 and 114 modules). A fast-event trigger was then formed (Chronetics 102) which indicated that an electron might have crossed within the momentum acceptance of the spectrometer. During

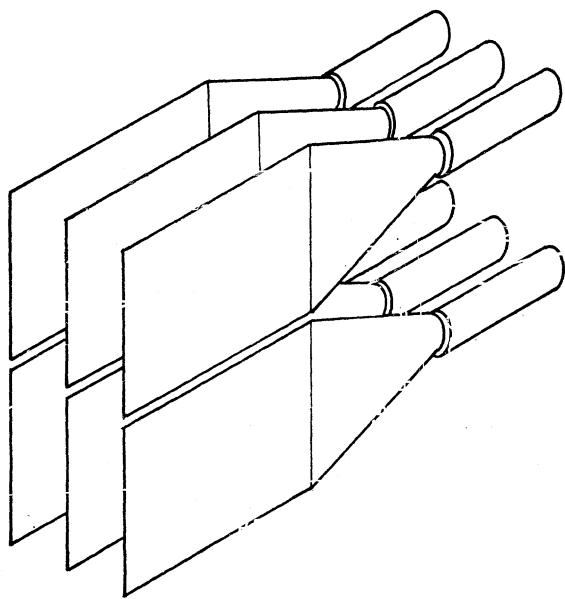


FIG. 6. Schematic perspective view of the proton counter telescopes.

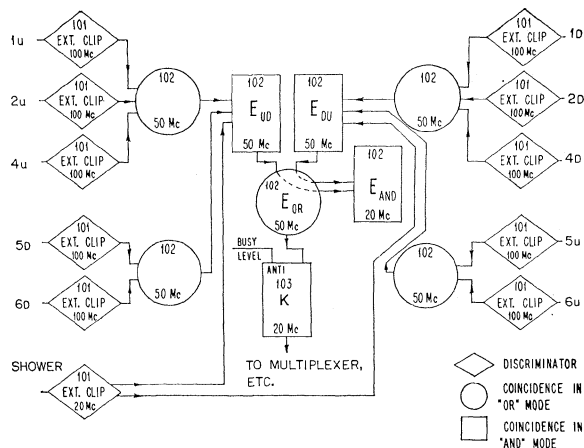


FIG. 7. Block diagram of the computer trigger. Numbers at the top of the frames indicate modulate numbers of Chronetics circuits and those at the bottom indicate the width settings of the circuits. The computer trigger is labeled "K".

this experiment two slightly different triggers were involved corresponding to a slight modification of the momentum defining array. The block diagram for the second of these is depicted in Fig. 7. The trigger was

$$E = (E_{UD}) \text{ OR } (E_{DU}),$$

where

$$E_{UD} = (1U \text{ OR } 2U \text{ OR } 4U) \text{ AND } (5D \text{ OR } 6D)$$

AND shower,

$$E_{DU} = (1D \text{ OR } 2D \text{ OR } 4D) \text{ AND } (5U \text{ OR } 6U)$$

AND shower.

The shower bias in this trigger was very low, ensuring better than 99.9% efficiency for electrons of the elastic scattering energy. The logic was designed so that events would generate a trigger even if one of the trigger counters was inoperative.

On generation of a trigger, fast gates recorded whether the discriminators associated with each and every counter had fired and this information was transmitted to a computer together with pulse-height information about the shower and Čerenkov counters and sundry other information. In addition, several fast coincidences were generated and their outputs scaled. These were used for independent checks of the functioning of the apparatus during data acquisition but played no role in the data analysis.

III. COMPUTER SYSTEM

The experiment was connected on-line to a PDP-1 time-sharing computer which served three main functions: (i) It performed certain checks on the apparatus which ensured that the electronic circuitry was operative (ii) it acted as a tape recorder, storing on magnetic tape all data transmitted to it, and (iii) it performed on-line data analysis which enabled the cross

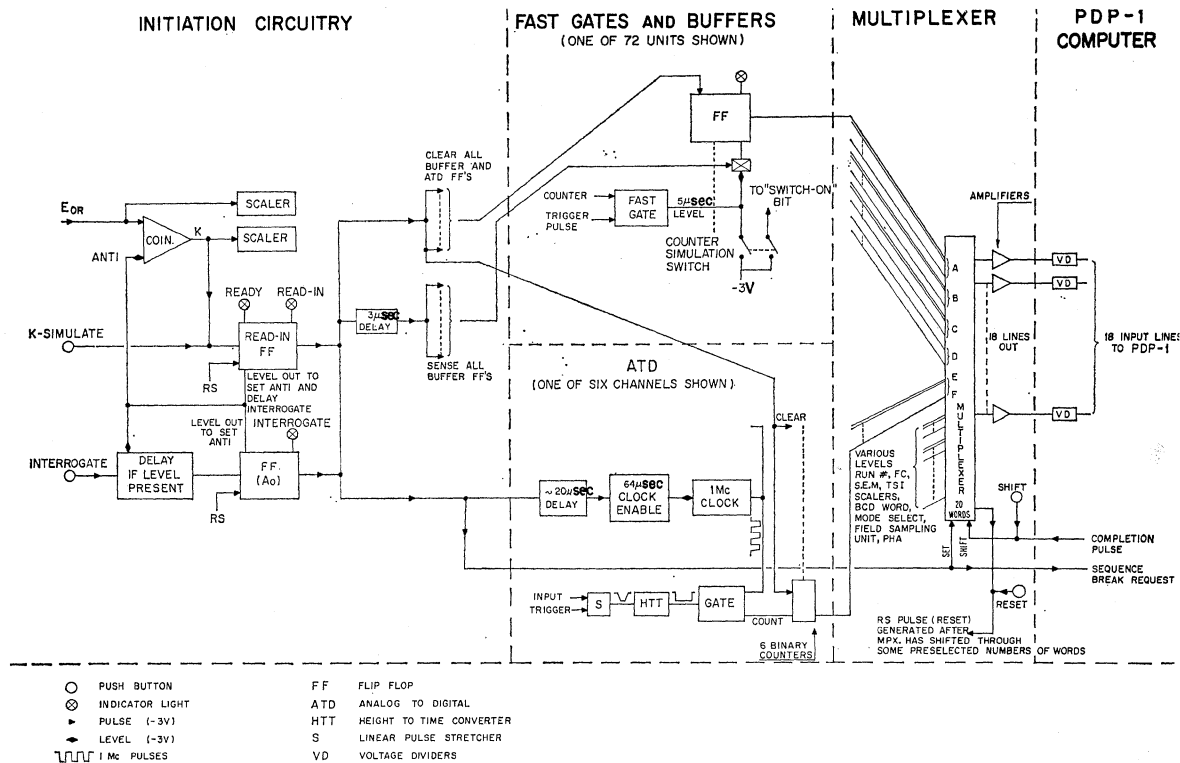


FIG. 8. Block diagram of the computer interface.

section to be evaluated with about 10% accuracy. The same program structure was used for the subsequent off-line data reduction, in conjunction with other arithmetic work performed on faster floating-point computers.

We refer the reader to Chap. 3 of Ref. 1 for the details of the computer system which can only be very briefly described in what follows.

The trigger to the computer was intended to be virtually 100% efficient for events of interest and was therefore made very nonrestrictive. In consequence, in the extreme case of the highest momentum transfer, elastic-scattering events constituted only 0.4% of all triggers. On receipt of a trigger, fast gates were interrogated to determine the state of all counter discriminators and, in addition, certain key counters such as the shower and Čerenkov counters were pulse-height analyzed. Other information connected with the event was also sampled. This included the charge collected during the run in the beam monitors, the field in the synchrotron magnets (this being a measure of the incident electron energy) at the time of the event, the current run number, and the value of one seven-digit scaler. In all, more than 200 bits of information were associated with each event and, in transmitting them to the computer, it was necessary to use buffers to "hold" the information and a multiplexer to transmit, one at a time, 13 words of 18 bits each. A schematic diagram of the interface logic is given in Fig. 8. The maximum

data acquisition rate, dictated by the computer, was one event per synchrotron burst. The maximum rate would then be 60 events per second but, in order that the sampled events be randomly picked from the machine spill, it was necessary not to exceed a rate of from five to ten events per second. In a few instances the beam intensity had to be reduced to achieve this.

The most important aspect of this procedure is that, since information is obtained and stored for each event individually, it is possible to examine in retrospect correlations between various parameters. In particular, one can subsequently analyze the data many times over with differing criteria (such as counter biases, momentum cutoff, presence or absence of coincident proton, etc.).

The analysis programs worked somewhat as follows: All information pertaining to an event was stored in a buffer area of core which, when filled, was transmitted to magnetic tape. Thus all data, regardless of the results of the on-line analysis, were stored. Each event was then analyzed. The analysis involved presentation of the event to a sequence of "filters." If the conditions imposed by any filter were not met, the event was not considered further. If all included filters were satisfied, the event was presented to a series of independent subprograms each of which performed some analysis on the event as a result of which some relevant histograms or storage words would be updated. Both during

and at the end of a run, the results of the analysis could be requested as displays on a storage oscilloscope which could be photographed.

Some of the filters were: (1) Require that each of the six pulse-height-analysis channels fall within a specified pulse-height "window" which could have upper or lower bounds, or both, (2) make some requirements on the momentum of the event (such as that it lie in some central group of momentum bins), (3) require that certain specified counter-firing patterns be present or absent (in particular, a bit corresponding to a coincident proton might be required to be on or off).

The analysis programs performed, in many instances, logic identical to that of the filters but, whereas the purpose of the filters was to determine the eligibility of an event for analysis, the analysis programs were responsible for the accumulation of the numerical results. Some examples were (1) determine whether the event was consistent with certain specified counter firing patterns. Each pattern thus was equivalent to a separate chain of electronic logic and the updating of the relevant storage location was equivalent to use of a fast electronic scaler; (2) momentum analysis of the momentum-defining counters (see Sec. IV B); (3) accumulation of histograms on each of the six pulse-height-analysis channels; and (4) creation of two-dimensional scatter plots for any two pulse-height channels.

The on-line programs, outlined above, were also used, with some few additional options, for the off-line data reanalysis. The discussions of Sec. IV bring out in greater detail the way in which these programs were used.

IV. DATA ANALYSIS

A. Survey of Data Analysis

We first survey the general scheme of the analysis in order to tie together the rather detailed accounts which follow. The basic detection was of electrons in the spectrometer which were in coincidence with a proton telescope count. A certain momentum bite about the central momentum for elastic scattering was selected and, subject to several corrections, the number of particles in that bite was taken to be the number of elastically scattered particles. Not all elastically scattered electrons fell into this bite and it was necessary to determine how many were outside it due, for example, to long tails of the resolution function and energy loss due to radiation. Moreover, it is possible for some electrons to be rejected incorrectly by the pattern recognition procedure used in determining the scattered momentum and thus not be accepted even though they actually were in the bite. These questions are discussed in Secs. IV B and IV M. Events can be included which are not due to electrons elastically scattered from hydrogen as well as elastically scattered electrons being missed. These might come from electrons involved in

inelastic pion production, electrons scattered from the aperture edges or pole face, electrons scattered in the target end walls, or from background processes which resulted in counter-firing patterns which looked like acceptable electron scattering events. An important question is the sensitivity of the results to the actual momentum bite taken. All these points are dealt with in Sec. IV C.

The efficiencies of the computer trigger, of the proton counters, and of the shower and Čerenkov counters are discussed in Secs. IV D, IV E, and IV F, respectively. The monitoring of the number of incident electrons is dealt with in Sec. IV G. The number of target protons depends on the length and density of the liquid-hydrogen target. Bubbling of the liquid hydrogen is a particularly troublesome problem. These matters are discussed in Sec. IV H.

Determination of the solid angle for detection of electrons is discussed in Sec. IV K. The cross section is a strongly varying function of the defining kinematic variables, here chosen to be the energy of the incident electrons and angle of the scattered electrons. These are discussed in Secs. IV I, IV J, and IV L.

The proton coincidence was not required in the computer trigger. Its presence was required, however, for the *cross sections* we present in Sec. V. We investigate the consequence of omitting the proton coincidence requirement in Sec. IV E.

The presentation of the results is deferred to Sec. V which also lists the errors in the measurements—the rationale for which is contained in the present section.

B. Momentum Analysis

The momentum analysis was a central feature of the data analysis and, as a result of the counter geometry, was somewhat unusual. It illustrates well the use of the computer to correlate several parameters. For these reasons we discuss this question in some detail.

(i) Trajectory Identification

The momentum-defining counter geometry has already been described in Sec. II C (iii). A typical firing pattern is indicated in Fig. 5. The ideal firing configuration can be spoiled by the failure of one or more counters to fire, or, more probably, by the firing of counters which are expected to be off. The pattern-recognition problem is handled in the following way.

A "mask" defines a so-called "perfect" trajectory for each momentum bin. It specifies all the counters which, in an ideal case, would fire and most of those which would not fire when a trajectory intersected the counter plane in the momentum bin in question. There are two masks for each of the 16 bins, one for falling (up-down) and one for rising (down-up) trajectories. Each event is compared with each mask in turn to determine the number of counters which would have to be turned off and turned on to match each mask.

TABLE III. Breakdown into categories of the momentum analysis. All events exceed certain shower and Čerenkov counter biases and are associated with coincident protons. Each category is presented as the percentage of the sum of 00, 01, and 10 categories (which provide a good measure of the "cross section"). An asterisk indicates a known malfunction of a counter. (Columns 3-7 are unambiguous.)

q^2 (F^{-2})	Fraction of triggers above final shower+ Čerenkov biases (%)	Fraction of codes 00+01+10 (in %)							Sum of preceding- four columns
		00	01	Unambiguous 10	02	11-22	Ambiguous all codes	77	
7	97.6	86.3	10.6	3.1	1.6	0.7	1.8	0.9	5.0
10	68	86.3	11.4	2.3	1.8	0.6	4.0	0.8	7.2
15	81	87	11	2	1.9	0.6	3.5	0.8	6.8
30	61	85	15	0.3	3	0.4	3.6	2.0	9
45	38	81	18	1	4	1.3	2.2	8	16
115	3.2	54*	45	1	10	1	4	11	26
130	1.9	82*	17	1	5	1.6	4	15	26
150	0.4	71*	13	16	3	9	2	6	20

A two-digit code is assigned to the comparison, the first digit being the number of counters which must be turned on, the second the number to be turned off. Thus the assignment "12" would imply one inefficient counter and two overefficient counters. If a "00" correspondence is established (complete agreement with a mask) the scan is halted since it has met with success. Otherwise all masks are scanned and then a decision is made as to how the event should be assigned. This is done on the basis that it is more likely that two counters be spuriously on (but less likely that three be on) than that one should be spuriously off. Thus events are assigned to that bin whose mask differs least from the event as determined by its having the numerically lowest of the possible codes: 00, 01, 02, 10, 11, 12, 20, 21, 22. If more than one bin has the same code and no other has one lower, the event is termed "ambiguous." It is assigned to the bin with that code first encountered in the scan. A separate count is kept of the relatively rare ambiguous events. If more than two counters must be turned on or off to obtain correspondence between the event and any of the masks, the event is considered unassignable (and given the code 77).

In practice, overefficient counters were a greater problem than inefficient counters. The dominant cause of overefficiency (a counter being on when it should be off) was not, as might be expected, due to random firing of counters due to backgrounds or noise—the frequency for which can be determined by delaying the counter signal so as to be out of time for real coincidences. It was found to be, in large part, correlated in time with the real signal.

We believe that this is due to the effect of knock-on electrons which are produced by interactions of electrons with the plastic scintillators through which they pass in describing a legitimate trajectory. Such a knock-on electron may then fire a neighboring counter

which would otherwise not have fired. We get excellent agreement between the observed frequency of such overefficiencies and calculation.

Table III indicates the frequency of the various categories of event for several momentum transfers. These frequencies are quite consistent with the known counter efficiencies and with the knock-on electron probabilities.

Finally, there remains to be discussed the vexing problem of the events which could not be analyzed by the pattern recognition program (termed code "77" events in the computer analysis). We present, in Table IV, a breakdown of these events. They are a more or less constant fraction of the elastically scattered electrons for all but the lowest momentum transfers (fourth column). (It should be remembered that the cross section varies over some seven orders of magnitude in these measurements.) Their number is not proportional to the total number of triggers (second column). Nor

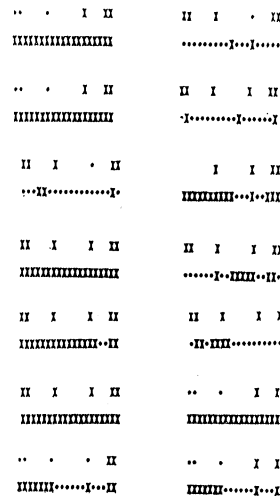


FIG. 9. First 14 code-77 events of a 45- F^{-2} run. A bias has been imposed on both the shower and Čerenkov counters, and there is a coincident proton. Each array is a computer-generated schematic rendering of the momentum defining counters. A large X indicates that a counter has fired. The target is to the left.

TABLE IV. Breakdown of code-77 events.

Code-77 events; with proton coincidence						
q^2 (F^{-2})	% of all triggers	% of triggers above chosen shower+ Čerenkov bias	% of codes 00+01+10	Number of code-77 events per 10^{-4} Coulomb of beam	% of all 77's above shower+ Čerenkov bias that have proton coincidence	
7	0.8	0.8	0.9	635	77	
10	0.5	0.7	0.8	210	83	
15	0.6	0.7	0.8	114	56	
30	1.0	1.6	2.0	24	73	
45	2.1	5.5	8.4	108	50	
115	0.2	7.5	11	2.5	18	
130	0.2	9	15	1.1	27	
150	0.02	4	6	0.2	24	

do they scale with the number of incident electrons (fifth column) which would allow for their interpretation as due to, for example, photon fluxes from the target. At $10 F^{-2}$, their proportion is the same whether the front or back apertures are used. At $45 F^{-2}$, there are less of them ($1.5 \pm 0.4\%$) when using the front aperture than when the back aperture is used ($5.5 \pm 0.5\%$).

These events are target associated as evidenced by their disappearance in empty target runs. Moreover, they display the same time distribution in the synchrotron spill as do perfect trajectories. On the other

hand, they do not, as a class, display the properties of elastically scattered electrons. The proton coincidences are a much smaller proportion of all code 77's (fifth column) than the 96% typical of perfect trajectories.

We discuss these events further for the particular case of $45 F^{-2}$. Figure 9 presents schematically the first 14 code-77 events of one of the data runs. The bottom two seem to be compatible with centrally crossing trajectories. However, the calculated probability for three counters to fire in coincidence with a crossing trajectory, including knock-on effects, is less than 0.2%. Moreover, in very "clean" situations such as the low-momentum-transfer runs, we do not see many such events, which confirms our suspicion that the large fraction of such events seen at high momentum transfers is not an inevitable characteristic of elastically scattered electrons.

In Fig. 10 we show scatter plots of the shower counter versus Čerenkov counter pulse heights for a $45 F^{-2}$ run. Plots of good trajectories (00 and 01 codes) and of nonanalyzable (77) events are shown (as well as codes 02 and codes 11 through 22, for interest). One clear feature is the large number of low pulse-height code-77 events. We are confident that these are of no concern since we know that electrons give large pulses in both the shower and Čerenkov counters. More worrying are those code-77 events whose shower and Čerenkov pulse heights are both large and fall in about the region into which the 00 and 01 events are grouped. We observe however, that these events show an average shower-counter pulse height somewhat lower (by about 15%) than that of the 00 and 01 codes. Moreover, there is a somewhat larger proportion of code 77's with high shower-counter pulses whose Čerenkov pulses lie in the overflow channel—which is what the Čerenkov response would be to the passage of several coincident particles. These observations are consistent with two explanations of these events: (i) Inelastically scattered

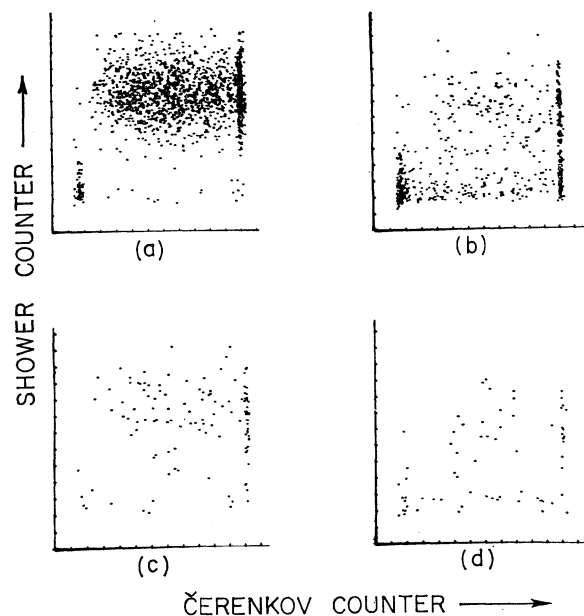


FIG. 10. Scatter plots of the shower counter (vertical) versus Čerenkov-counter pulse height (horizontal axis) for certain classes of events at $45 F^{-2}$. (a) codes 00-01; (b) code 77; (c) code 02; (d) codes 11-22.

TABLE V. List of contributions to the momentum resolution. The situation depicted is for a 2-in. target. The numbers quoted are estimates of the contributions to the full-width at half-maximum assuming a focus near the central momentum bins. p is the momentum, in BeV/c, of the scattered particle and s is the average slope of trajectories in the quadrupole, here taken to be $1/28$.

Source	Theoretical estimate (%)	Calculated effect (%) at		
		1.5	3.0	4.5 BeV/c
Target				
beam height	1.0	1.0	1.0	1.0
target length	1.47	1.47	1.47	1.47
Before quadrupole, target and other material	$(15/p_s) \times 0.81$	0.227	0.113	0.076
Quadrupole, aberrations and kinematic smearing	0.7	0.7	0.7	0.7
After quadrupole, multiple scattering in counters	$(15/p_s) \times 1.23$	0.344	0.172	0.115
Total (adding in quadrature)		1.95	1.92	1.92

electrons will focus before the momentum counters, passing through either all "up" counters or all "down" counters and may fire some other counters by knocking-on electrons or by some other mechanism. (ii) Scattered charged particles may strike the pole faces or plug in the magnet or the rear aperture edge, shower, and produce a spray of particles. The first possibility provides an explanation for the lower number of 77's at low momentum transfers since the inelastic electron threshold is then far from the elastic momentum. Both explanations are in agreement with the approximate scaling of the code 77's with the elastic cross section.

While the type of argument given above is suggestive, one cannot necessarily assume that all code-77 events belong to the same class of events. There may be some fraction of them which are associated with genuine elastically scattered electrons passing through the aperture. We have "hand-scanned" the code-77 events and find some fifth of them, viewed by subjective criteria, could *conceivably* be "good" events. This proportion holds for both the high momentum transfers and for the relatively less numerous code-77 events at the low momentum transfers. We have, therefore, taken one-tenth of the code 77's to be acceptable events and assigned an error equal to the number accepted. This introduces a typical error of $\pm 0.75\%$ in the intermediate momentum-transfer range which is a very large error for a measurement of this kind. It suggests that a radical redesign of the spectrometer would be required to perform absolute cross-section measurements to much better accuracy than that of the present experiment.

(ii) Events Shifted In and Out of Bite Taken

Inefficiency or overefficiency of a counter can result in assignation of events with a "00" code to the bin adjacent to the one in which the true trajectory passed. One effect of such bin shifting is to add slight tails to

the resolution function. One might worry that the number of events in the acceptance bite might be significantly altered by this effect. However, there is a cancellation between rising and falling trajectories provided the cutoff is in a reasonably smoothly varying region of the momentum spectrum, which is normally so. The uncertainty is then of the order of a few percent of the difference between the number of up-down and down-up events in the momentum bins in the region of cutoff. This leads to a typical error in the cross section of less than $\pm 0.2\%$.

(iii) Momentum Resolution

The importance of knowing the momentum-resolution function is twofold: First, in order to be able to estimate the fraction of elastically scattered electrons excluded from the acceptance bite by virtue of being in the tails of the resolution function; and second, in order to determine whether events observed either side of the elastic peak are due to the natural tails of the resolution function or to background contamination (which would presumably also be present under the peak).

Calculated estimates of the momentum resolution are presented in Table V, which gives an idea of the importance of various contributions. The shape of the momentum resolution was expected to be roughly Gaussian, with perhaps somewhat smaller than Gaussian tails. In practice the observed peak width agreed with the calculated values to about $\pm 0.4\%$ FWHM, but was found to vary by about that much from day to day. This is not clearly understood, but is thought to be due to fluctuations in the vertical beam position which would lead to a time-averaged beam profile which would be broader than that observed in a short-term glass-slide exposure. Moreover, there was a high momentum tail to the resolution function, especially marked for down-up trajectories. This tail was present

even at very low momentum transfers where background contamination is negligible and hence is clearly established as intrinsically due to acceptable elastically scattered electrons. It is thought to be due to some effect such as the presence of knock-on electrons as described above in Sec. IV B (i). These would affect down-up trajectories preferentially, but our calculations do not predict as large a tail as was observed.

Because the effects observed were not completely determined by calculation and the resolution width was not predictable on the basis of the monitored parameters, the resolution function in each case was obtained by scaling, to fit the data, curves which, when radiative effects were allowed for, fit the "clean" low-momentum-transfer data.

One final, very puzzling feature of the observed resolutions is that, at several momentum transfers, the widths of the peaks produced by rising and by falling trajectories were appreciably different. We can find no explanation for this effect. It was not due to multiple-scattering broadening which was only slightly different for the two trajectories. One possibility we considered is a different dispersion for the two trajectories due, for example, to a tilt of the counter array out of the horizontal plane. To produce the observed effect such a tilt would be of the order of $\frac{1}{2}$ in. over the entire array, which is very large indeed. However, such an explanation is ruled out since it results in radically different ratios of inelastic electroproduction to elastic scattering cross sections for the two trajectories.

This anomaly is unfortunate mainly because it is not understood. Its effect on our results is, however, expected to be small. This is because there is a good cancellation between up-down and down-up corrections in all instances in which the width of the resolution function or the momentum dispersions are of concern.

C. Contamination by Nonelastic Events

(i) Empty-Target Subtraction

The end walls of the target were made of 0.0015-in. aluminum and were responsible for a few percent of the accepted scattered electrons. Moreover, it is possible that there were other sources of scattering such as the copper feed lines between the cryostat and target cup which could conceivably interact with any beam halo present. Data were therefore taken with the target evacuated. The electron arm rate in a $\pm 3.5\%$ momentum bite was always consistent with $(6/t)\%$ of the target full rate, where t is the target length in inches and was typically between 1.2 and 3.5 in. The electron-proton ($e-p$) coincidence rate in the target-empty runs was always equal to one-third of the total electron rate to within the accuracy of the measurement. The subtraction was of $e-p$ coincidences and was therefore a $(2/t)\%$ subtraction. These rates were con-

sistent with calculations of the rates due to scattering by the target walls.

At momentum transfers above 70 F^{-2} , the expected number of empty target $e-p$ coincidences was small or zero due to the low counting rates. Empty-target runs were still made, but were viewed as *checks* on the data. The subtraction made was the $(2/t)\%$ subtraction inferred from the more accurate low-momentum-transfer data.

(ii) Events Above Peak

At a given scattering angle with a monoenergetic electron beam, no particle has a higher momentum than an elastically scattered electron. Thus, the momenta above the elastic peak are kinematically forbidden and, ideally, there would be no events there. Possible sources for legitimate events are electrons scattered from nuclei in the target and walls and particles associated with long tails of the resolution function. The former should be excluded by an empty-target subtraction. The latter are reasonably well known from the low-momentum-transfer data. We have estimated the number of events which would lie under the elastic peak if those events observed above the peak, and not accounted for by the above effects, are associated with a flat momentum spectrum extending to low momenta. We subtract one-half the contamination suggested by such above-peak events and assign an error equal to the subtraction.

The fraction of events thus subtracted is very small, being 0.2, 0.6, and 1.5% of the elastic peak events at 115 , 130 , and 150 F^{-2} , respectively, and less than 0.1% below 115 F^{-2} . These numbers are a good indication of the scale of possible contamination, and are satisfactorily small.

(iii) Charged and Neutral Pions and Protons

Charged pions and protons are produced in the target. Particles produced in the hydrogen should have reduced momenta compared with elastically scattered electrons and should also have pulses below the bias levels in the shower and Čerenkov counters. We have estimated the contamination by such particles to be less than 0.2% of elastically scattered electrons in the worst case (150 F^{-2}).

Neutral pions do not, of course, count directly but can register by virtue of their Dalitz decay which produces an electron-positron pair. We have calculated the possible contamination and find it to be less than 0.1% in the worst case (150 F^{-2}).

(iv) Electropion Production

A major source of contamination is from electrons involved in single pion production, one prominent feature of which is the excitation of the first (1236-MeV) nucleon resonance. The two reactions are

- (a) $e+p \rightarrow e+p+\pi^0$,
- (b) $e+p \rightarrow e+n+\pi^+$.

TABLE VI. Comparison of Adler theory with data. Momentum transfers are those of elastic scattering kinematics. We give our calculated elastic cross section and that of Adler's inelastic calculation evaluated at an excitation (shown) near, but not actually at, the peak of the N^* . The Adler cross section is the electron-only detection from both $e+p \rightarrow e+p+\pi^0$ and $e+p \rightarrow e+n+\pi^+$. We show, for up-down and down-up trajectories separately, two comparisons: (1) the ratio of N^* observed to be produced to the Adler prediction (this is an average over the region extending from threshold to just about the N^* peak); (2) the ratio of the fraction of observed inelastic electrons which have a coincident charged particle to the theoretically predicted fraction.

Elastic q^2 (F^{-2})	N^* electron only ud	Ratio data/theory du	Fraction ($e+p$)/ e ud	Ratio data/theory du	Elastic cross section corre- sponding to form factors used for the N^* (10^{-32} cm 2 /sr)	$E_{c.m.}^*$	Adler prediction for N^* produc- tion at $E_{c.m.}^*$ $\mu\text{b}/(\text{sr BeV})$
45	2.0	1.6			0.5635	1236	0.01973
70	2.1	2.4			0.1030	1224	0.00342
75	2.7	2.9	2.2	1.9	0.0897	1247	0.00245
90	2.5	1.9	1.9	1.3	0.0305	1247	0.000848
100	2.3	2.4	0.9	1.3	0.0118	1245	0.000363
115	3.5	2.4	2.4	2.8	0.00634	1247	0.000185
130	3.1	2.7	2.4	2.8	0.00271	1247	0.0000828
	Cone data (see Ref. 6)						
30		1.4					
45		2.0					
100		1.7					

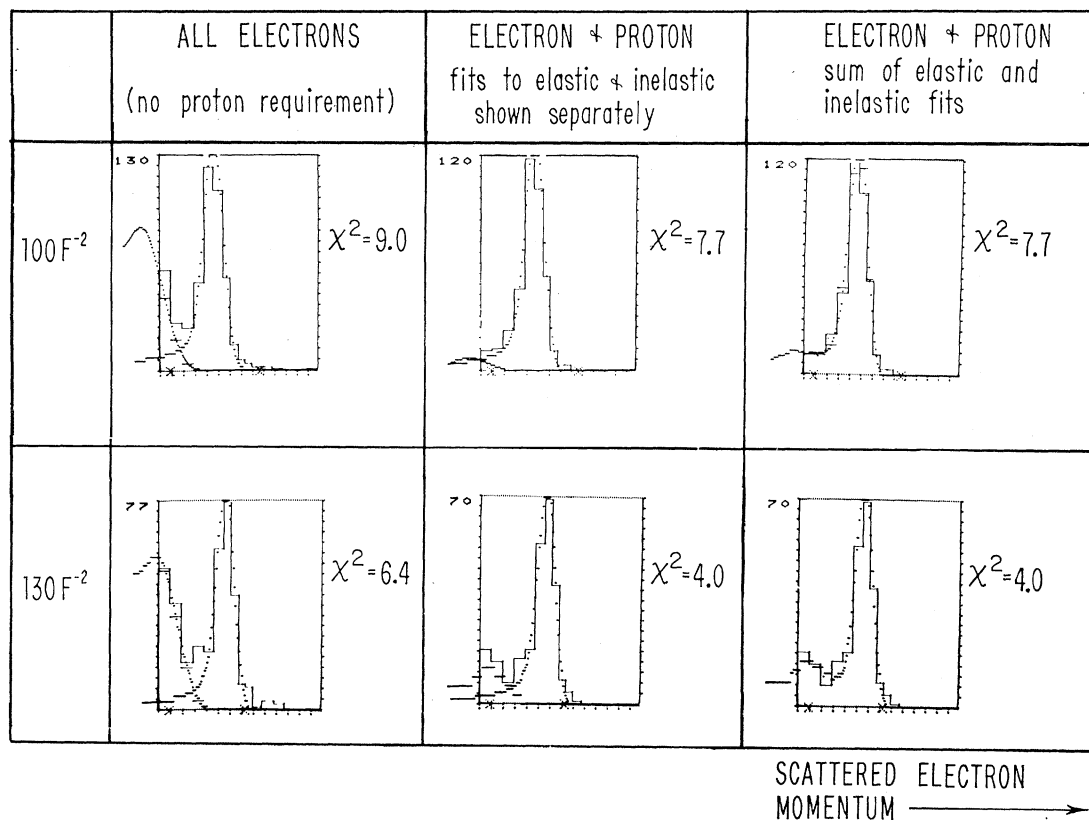


FIG. 11. Comparison of the data with estimates of the resolution function and of inelastic electroproduction. Radiative corrections are included. The bar histogram is the data, the dotted curves are the theoretical fits, and the horizontal lines are the integrals of the theoretical fits over the experimental bin widths. The number at the top left of each graph is the full scale value of the y axis. The χ^2 evaluation is at the right of each plot. There are six degrees of freedom in the fits.

Such inelastically scattered electrons have a continuum of momenta below a threshold momentum whose separation from the elastic scattering momentum scales inversely with incident electron energy. The worst case is at 6-BeV incident energy, when the threshold is only 2.3% below the elastic peak. Our modest momentum resolution then implies the possibility of a serious contamination from inelastically scattered electrons within a momentum bite large enough to accept the bulk of elastically scattered electrons.

Coincident detection of a charged particle at or near the angle at which protons recoil from elastic collisions reduces, but does not eliminate, the contamination. Near threshold, reaction (a) is suppressed and S -wave charged-pion production (b) dominates. The charged pions are indistinguishable, in this experiment, from protons but are spread out over quite a large cone, only a portion of which is subtended by the coincidence-counter telescope.

To estimate the contamination, one must know the shape and magnitude of the scattered electron momentum spectrum near threshold, both with and without coincident charged-particle detection. To obtain this, we used the dispersion theory of Adler⁸ to estimate the cross sections of both reactions (a) and (b) above, differential in electron scattered energy and solid angle and in pion solid angle. We then integrated these predictions over the coincidence-counter acceptance, and also, separately, over all pion angles, to obtain the electron momentum spectrum with and without coincident charged-particle detection, respectively.

In comparing these theoretical spectra with the data, it was clear that the theory was substantially underestimating the cross section at high momentum transfers. Thus it was not possible to use the theory to calculate the contamination directly. Instead, it was assumed that the *shapes* of the spectra were correct and their magnitudes were adjusted to fit the observed data. The fitting procedure was complicated⁹ because it was necessary to fold in the resolution function and to include radiative corrections which distort all the spectra. In addition, the width of the resolution function was considered a variable, as discussed in Sec. IV B. From the best fit, the contamination in the acceptance bites was estimated. Since the theory is in some doubt, we assign a conservative error of one-half the correction made in each instance.

Table VI indicates the observed ratio of experiment to theory for the various data points. The two trajectories were treated separately and somewhat different results were obtained for each. We show both ratios separately and suggest that the error in the determination is probably of the order of the discrepancies be-

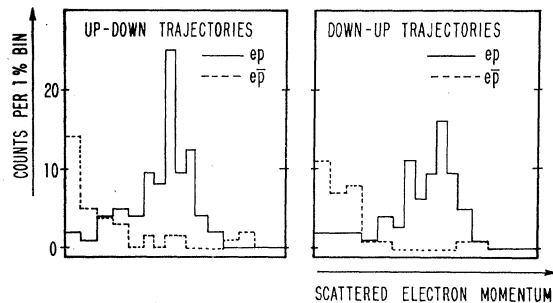


FIG. 12. Momentum spectra of electrons at $150 F^{-2}$. Continuous lines are of electron-proton coincidences, dotted lines are of electrons with proton anticoincidence. The inelastic contamination was taken to be one-third of the $e\bar{p}$ spectrum, making allowance for a 4% proton inefficiency for elastic scattering.

tween the two trajectories. We, in fact, compared the ratio of inelastic to elastic electron scattering in the data to that same ratio in theory, thereby considerably reducing the sensitivity to the values assumed for the form factors. We also show the same ratio as observed by Cone.⁶ The agreement between our two experiments is quite satisfactory. We also give the calculated inelastic cross section at the peak of the $\Delta(1236)$ resonance (differential in electron energy and solid angle) together with the elastic cross section in order that others may reproduce our results. Difficulties with Adler's predictions at high momentum transfers involving electropion production from *neutrons* are discussed by Budnitz.²

Figure 11 shows typical fits, as described above, for up-down trajectories at 100 and 130 F^{-2} . The computer generated displays show the electron-only momentum spectra and the $e-p$ spectra, which involve the coincident detection of a charged particle. In the latter case the fits to the elastic and inelastic spectra are shown individually and in sum in separate displays for purposes of clarity.

The procedure followed at 150 F^{-2} differed from that described above. This was because the paucity of data did not allow a meaningful fit. What was done was to extrapolate the ratio of electron-proton coincidences ($e+p$) to anticoincidences ($e\bar{p}$) found experimentally at lower momentum transfers. The measured $e\bar{p}$ spectrum at 150 F^{-2} was then used in conjunction with this ratio to predict the $e+p$ inelastic spectrum. Figure 12 shows the measured and deduced spectra for about half of the 150- F^{-2} events.

(v) Sensitivity of Cross Section to Momentum Cutoff

It is important that the cross sections not depend critically on the point at which the low-momentum cutoff is taken. The fits of Fig. 11 contain the information of concern but we have explicitly plotted the cross section as a function of the cutoff for a few momentum transfers in Fig. 13. The stability is very satisfactory.

⁸ S. L. Adler, Ann. Phys. (N.Y.) **50**, 189 (1968); and private communication.

⁹ See Sec. 4.3.e of Ref. 1.

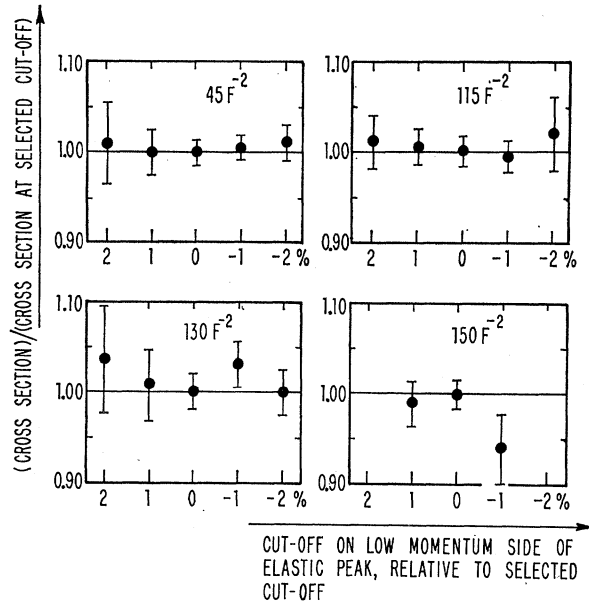


FIG. 13. Cross-section dependence on low-momentum cutoff, at 45, 115, 130, and 150 F^{-2} . The ratio of the cross section which would be obtained relative to that at the selected cutoff is plotted against the cutoff (measured relative to the selected cutoff in % of the elastic momentum). The sum of up-down and down-up trajectories is involved. The errors are the relative errors of the points and do not include statistical errors. They are obtained from the combination of one-half of the inelastic electroproduction contamination and one-fifth of the contents of the last included bin (to include errors from bin shifting, etc.).

D. Apparatus Dead Times

(i) Trigger Dead Time

Dead times in the trigger counter discriminators and in some subsequent electronic circuits lead to trigger inefficiencies of as much as 1.5% in the worst case. Unfortunately, the dead-time characteristics of the circuits were inadequately appreciated in the initial stages of the experiment and, as a result, the parameters on which the dead times depended were poorly monitored and there are consequently uncertainties of as much as the amount of the correction itself.

(ii) Computer Dead Time

The computer had a dead time which resulted in the number of events recorded on tape being less than the number of triggers generated. The latter quantity was, however, scaled so that this dead time could be corrected for exactly, provided only that the triggers accepted were a random sample of all triggers. To achieve this, the computer dead time was kept below about 5% by lowering the beam intensity when necessary.

E. Proton Counter Efficiency

(i) Setting and Monitoring of the Gains

The gains of the proton counters were set by determining their efficiency in what amounted to a tagged-

proton beam, namely a beam of recoil protons associated with well-defined elastically scattered electrons detected in the electron spectrometer and guaranteed to strike the proton counter by virtue of the kinematics of elastic scattering. "Clean" electrons were obtained by requiring high shower and Čerenkov pulses, unambiguous trajectories on the top of the elastic peak, and by operating at fairly low momentum transfer (30 F^{-2}), where background processes were negligible.

(ii) Comparison of Measured and Calculated Proton Counter Efficiencies

By selecting clean electrons as just described, from the actual data runs, it is possible to *measure* the proton counter efficiencies. However, there is the possibility that the measurement will degenerate at high momentum transfers if the electron arm ceases to be self-sustaining. On the other hand, one can calculate the expected efficiency taking into account (i) proton losses due to wide-angle scattering in the target and the air path between target and counters; and (ii) the loss of protons due to nuclear absorption in the air and within the counters themselves. Table VII lists the measured and calculated proton counter inefficiencies. Agreement is, in general, good and the slightly low calculated inefficiency at high momentum transfers is thought to be understood, at least in part, by omission of inelastic contributions to the absorption cross section.

(iii) Role of Proton Counters in Data Analysis

At momentum transfers of 70 F^{-2} and below the measured efficiency [as described in (ii) above] was used to extract the cross section. The use of the *measured* efficiency in this way has several ramifications: The efficiency measurement is based on a subset of all eventually accepted events which usually corresponds to about 70% of them. This subset is, in effect, accepted without the requirement of a proton coincidence. The

TABLE VII. Comparison of calculated and observed proton-counter inefficiencies.

q^2 (F^{-2})	Calculated inefficiencies (%)	Proton-counter inefficiencies (%)	
		Observed (%) Up-down	Down-up
7	4.51±0.5	4.8±0.3	4.0±0.3
15	4.89±0.55	6.9±0.3	5.1±0.3
30	1.89±0.35	2.4±1.2	0.1±1.4
45	2.04±0.4	0.8±0.6	1.2±0.7
70	2.02±0.4	2.7±1.5	6.1±1.7
75	1.9±0.8	2.5±8	7.7±6
100	1.9±0.8	5.3±1.5	5.0±1.6
115	1.9±0.8	1.0±3	5.9±3.6
130	1.9±0.8	4.4±5.7	0(4)±3.2
150	1.9±0.8	5.4±13	0(3)±29

coincidence is only imposed on events falling short of perfection due either to low pulse heights in the shower or Čerenkov counters, nonperfect trajectories, or because they lie in the tails of the elastic peak. The error in the proton efficiency is thus only applicable to the 30% or so of events not used in its determination. Moreover, effects due to random coincidences in the proton counters or gain shifts due to instantaneously high beam intensities are directly measured by our technique and, therefore, introduce negligible error into the determination of the cross section.

At $75 F^{-2}$ and above, the proton coincidence was required of all accepted events. We do *not* use the measured efficiency but, rather, assume an efficiency of $97.5 \pm 1\%$. This is lower by $\frac{1}{2}\%$ than the calculated value but is consistent with the measured values at the lower-momentum-transfer points where better statistical accuracy was possible. This discrepancy is considerably less than the statistical errors involved in the cross-section measurements.

(iv) *Effect on Cross Section of Removing Proton Coincidence Requirement*

Requirement of a proton coincidence should be kinematically redundant. It is a vital check on the experiment to determine what results would be obtained if the proton coincidence were not invoked.

Table VIII shows, for some of our data, the changes in our estimates of the cross sections which would result from ignoring the proton coincidence in selecting

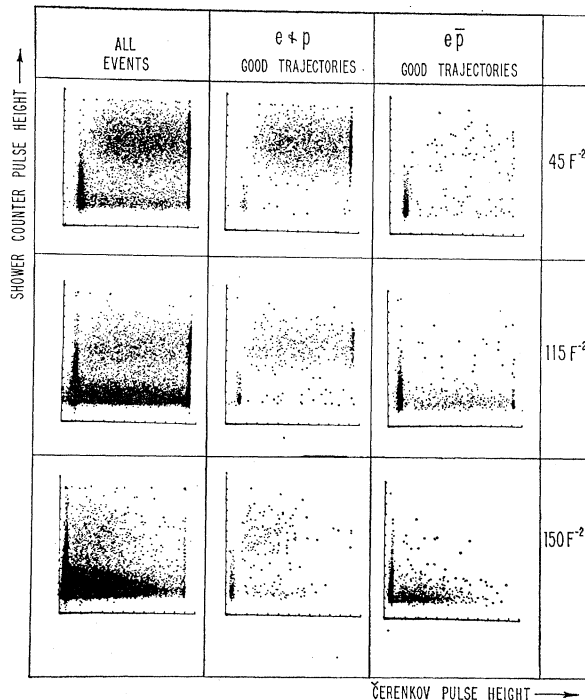


FIG. 14. Scatter plots of the shower counter (vertical) versus Čerenkov counter (horizontal axis) at 45 , 115 , and $150 F^{-2}$. See text for details.

TABLE VIII. Effect of removing the proton coincidence requirement at the high momentum transfers. The ratio of the cross section which would be obtained if no coincident proton is required to the cross section with coincidence is shown for the high momentum transfers. The errors quoted are relative errors and derive almost entirely from the increased inelastic contamination when no coincidence is required. Below $75 F^{-2}$ the measured proton efficiencies were used and the ratio of this table is then not more than 1% different from unity, with no more than 1% uncertainty at $45 F^{-2}$ and below.

Momentum transfer (F^{-2})	σ (electron only) $\sigma(e+p)$
90	1.02 ± 0.06
100	1.06 ± 0.06
115	0.996 ± 0.05
130	1.03 ± 0.06
150	1.02 ± 0.06

scattered electrons. (The proton counters are, however, still involved in estimating the Čerenkov counter efficiency—see Sec. IV F.) To within the accuracy of the comparison the measurement is not altered by relaxing the proton coincidence requirement. This gives us great confidence in our coincidence results.

F. Shower and Čerenkov-Counter Efficiencies

(i) *Shower versus Čerenkov-Counter Scatter Plots*

We present, in Fig. 14, scatter plots of the shower versus Čerenkov-counter pulse height at momentum transfers of 45 , 115 , and $150 F^{-2}$. At each momentum transfer, we show scatter plots of all triggering events (labeled “all events”); events with good trajectories (codes 00 and 01) in the accepted momentum bite which had a proton coincidence (labelled $e+p$); and good on-peak trajectories which had no problem coincidence ($e\bar{p}$).

The most important point to observe is the excellent separation of electrons in the $(e+p)$ plots which persists up to the $150 F^{-2}$ data. Up to, and even including, the $115 F^{-2}$ data, a bias in the shower counter alone would provide adequate separation. Above $115 F^{-2}$ a bias in the Čerenkov counter is also necessary. The $e\bar{p}$ plots demonstrate the role of the proton coincidence in cleaning up the measurement. The few $e\bar{p}$ events with large shower and large Čerenkov pulses are mainly associated with the proton counter inefficiency which is of the order of $2\frac{1}{2}\%$. The number of $e\bar{p}$ events with low shower or Čerenkov pulses, or both, becomes very appreciable as the momentum transfer increases. We present the (all-events) plots to indicate how the trigger deteriorated as momentum transfer increased.

(ii) *Sensitivity of Cross Sections to Shower and Čerenkov-Counter Bias*

Biases for the shower and Čerenkov counters were chosen on the basis of an inspection of these scatter

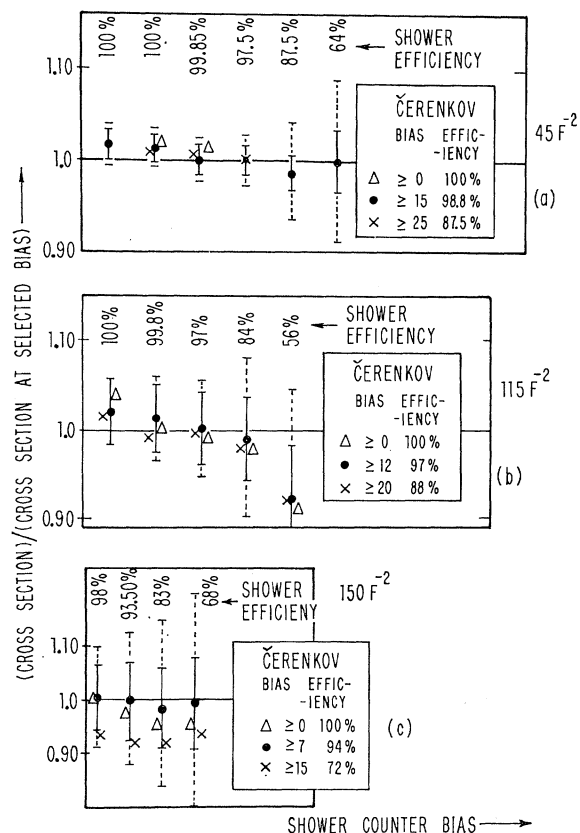


FIG. 15. Cross section as a function of bias in shower and Čerenkov counters at 45, 115, and 150 F⁻². The ratio of cross section at a given bias to that found at the bias eventually chosen is plotted against the lowest channel accepted in the shower spectrum. Three different Čerenkov biases are plotted in most instances, the lowest being the case in which the Čerenkov counter is not required at all (channel 0). The solid error bars are the result of statistical uncertainty in the cross-section determination and in the determination of the shower and Čerenkov efficiencies. The dotted lines are estimates of the uncertainty in the determination of the efficiencies based on the possibility of drifts in the ATD gains.

plots and the data were analyzed with the selected biases and also with both higher and lower biases to ensure that the results were insensitive to the bias chosen. Figure 15 shows the results of such determinations at 45, 115, and 150 F⁻². The stability for rather wide ranges of biases is a good indication that the counter efficiencies are understood. More importantly, it suggests that our results are relatively free of contamination from backgrounds such as charged pions since the proportion of events from such processes would be expected to decrease rather rapidly with increasing level of bias.

(iii) Shower-Counter Efficiency

The shower counter, with a rather low bias, was a constituent of the computer trigger. Inspection of the spectrum of pulse heights of all events resulting in a trigger indicates at least 99.9% efficiency of this low

bias for all data reported here. However, higher biases were imposed in the data analysis. The efficiency was determined as follows.

Events were selected from the *data* runs with the characteristics of having coincident protons, large Čerenkov pulses, and perfect (codes 00 or 01) on-peak trajectories. The response of the shower counter to these clean electrons was then determined. At and below 30 F⁻² the pulse-height spectra of such events is quite clean, showing no sign of background contamination. This technique is then considered as *measuring* the shower-counter efficiency. At higher momentum transfers a small amount of background begins to appear in the low-energy tail of the spectrum. At 150 F⁻² this background is as much as 20% of all such events.

Above 30 F⁻² the shower-counter efficiency was determined by comparison of a pulse-height spectrum obtained in a clean situation (10 F⁻²) with a spectrum obtained as described above. The underlying assumption was that the low-momentum-transfer spectrum was a good representation of the shower-counter response to energetic electrons. The only difference would lie in a somewhat different scale and absolute gain. These were adjusted by comparison with data at the correct scattered energy. A typical example of this comparison is shown in Fig. 16.

The uncertainty in the efficiency was taken to be the change in efficiency which would result from one-half a channel change in bias.

(iv) Čerenkov Counter Efficiency

At momentum transfers of 100 F⁻² and below, the efficiency was obtained from the data runs looking at

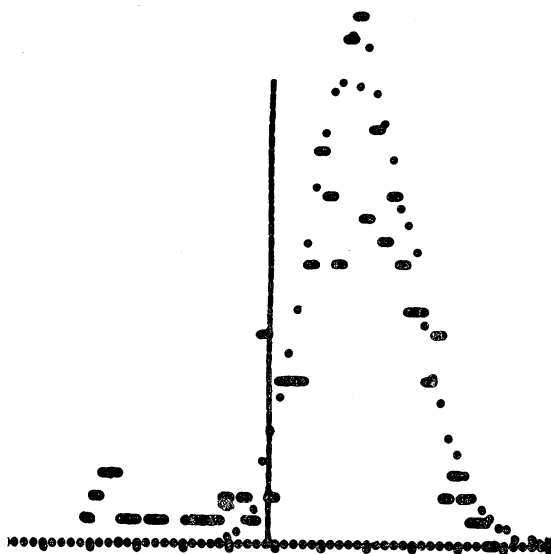


FIG. 16. Comparison of shower counter spectrum from a 115-F⁻² data run (horizontal bars) with a scaled 10-F⁻² spectrum (dots). The vertical scale and the horizontal scale and displacement are varied until the minimum χ^2 is achieved. The χ^2 is evaluated for points to the right of the vertical line.

events with a high shower-counter pulse, coincident proton, and perfect on-peak trajectories. The effect of this method was that the Čerenkov counter was effectively not used in accepting the fairly large class of events used to determine its efficiency. It was only used in screening the more dubious events with, for example, imperfect momentum-defining counter patterns.

At and above 115 F^{-2} , a Čerenkov-counter bias was required of *all* events. The efficiency was then determined by a technique very similar to that already described for the shower-counter efficiency determination at high momentum transfers. The difference was that the clean spectrum was not taken from a low-momentum-transfer data run, but from a calibration run taken in conjunction with all high-momentum-transfer runs. In these calibration runs, electrons of the same incident energy as used in the data runs were allowed to hit either a hydrogen or polyethylene target. The electron arm was moved to a forward angle (about 12°) and the spectrometer was set to detect inelastically scattered electrons of the same scattered energy as would be associated with elastic scattering at the high momentum transfer. In this way a high counting rate and a relatively good electron-to-background rate were obtained without having to alter the synchrotron energy. Events with a high shower-counter pulse and a perfect trajectory in a momentum bin corresponding to the position of the elastic peak in the data runs were selected. The efficiency thus obtained was always consistent with that determined from the clean-data events, but had better statistical precision.

G. Number of Incident Electrons

(i) Faraday Cup Efficiency

A Faraday cup provided the absolute monitor of the charge in the beam. The basic design of this cup, CEA Faraday cup No. 2, has been discussed by Burr.¹⁰ The calculated efficiency of the cup is better than 99.9%. Measurements of the response of the cup relative to some secondary monitor as the potential of the cup relative to its outer casing is varied are relevant to the determination of efficiency. Typically, plateaus were obtained at large positive and negative biases which differ by $+0.15$ and -0.3% , respectively, from the response at zero bias (where the data runs were taken). Some hold that these plateaus represent the extremes within which the 100% efficiency point must lie. Others prefer to consider the apparent variation of efficiency with bias as a symptom which suggests a scale for possible malfunction of the device without being an absolute indication of its accuracy.

A further measure of the efficiency has been made using a toroid coil to detect directly the difference between the charge in the beam and that collected in the

cup. A preliminary determination gave¹¹ an efficiency of $99.2 \pm 0.4\%$. We have, however, taken the Faraday cup (at zero bias) to be $100 \pm 0.25\%$ efficient, based primarily on the bias curve measurements. We consider that the toroid measurement is not yet sufficiently well understood. We do consider that it offers an important *check* at the 1% level on our assumed value for the efficiency.

A recent comparison of Faraday cups used at the Cambridge Electron Accelerator¹² and at SLAC concluded that their efficiencies were identical to within the measurement error of 0.3%. Since the design of the cups is basically the same, this is no surprise. Losses due to Coulomb scattering out of the beam were calculated to be less than 0.1%. At low energies a helium bag was used to reduce these further. The response of the Faraday cup relative to a secondary monitor was unaffected by ± 1.5 -in. movements of a 5-BeV beam.

(ii) Faraday Cup/Secondary Emission Monitor Ratio

The secondary monitor was CEA secondary emission monitor No. 4. During data runs, the ratio was almost always constant to within 1%. Moreover, agreement between runs at different dates is good. We regard this ratio as providing a check at the 1% level of our absolute monitor stability together with that of the integrators.

(iii) Integrator Calibration

Before or after each run the integrators were calibrated by depositing a known charge into them. Two separate calibration devices and an intercalibration with a CEA integrator confirm that our integrators were accurate to within $\pm 0.1\%$ for collection of charge involving at least 100 cycles. The 24-h stability was well below 0.1% drift.

H. Length and Density of Target

(i) Target Length Measurement

The targets ranged in length from 1.2 to 3.5 in. The lengths were measured at room temperature by mechanical techniques to an accuracy of better than 0.002 in. Compensation was made for changes in length due to the low temperatures of operation and to the pressure differential between the inside of the cup and its vacuum environment. The corrections amounted generally to a few tenths of a percent. The main uncertainty in target length arose from the rough treatment occasionally meted out to the target cups which resulted, in the worse case, in a $\pm 0.9\%$ uncertainty in target length.

¹¹ G. F. Dell, J. dePagter, M. Fotino, H. Holcomb, and L. Law, in Proceedings of 1966 International Conference, Instrumentation for High-Energy Physics, p. 597 (unpublished).

¹² G. F. Dell, and M. Fotino, CEA Report No. CEAL-1043 (unpublished).

¹⁰ P. H. Burr, CEA Report No. CEAL-1008 (unpublished).

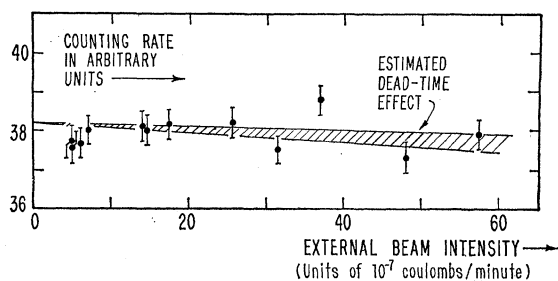


FIG. 17. Intensity dependence of the cross section.

(ii) Beam Position in Target

Off-center displacements of the beam and the small angle which the beam may make with the target axis affect the interaction length. The bulge of the end walls involves additional corrections for angles coupled with corrections for off-center displacements of the beam. Moreover, the lateral extension of the beam involves integration over a small range of lengths weighted by the distribution function of the beam profile. In practice these corrections were always less than 0.15%.

(iii) Density of Liquid Hydrogen

The density of hydrogen was taken to be¹³ 0.0351 g molecules/cm³ at 760-mm Hg.

As described in Sec. II B, the temperature of the liquid hydrogen was deduced from the pressure at its surface which was monitored to better than ± 25 mm Hg, leading to a $\pm 0.14\%$ uncertainty in the density.

(iv) Boiling and Bubbling—Beam Independent

The aforementioned errors are overshadowed by the problem posed by the possibility of bubbling in the target which clearly lowers the effective density. There are two types of problem: beam-associated and beam-independent bubbling.

Beam-independent bubbling arises from the absorption of radiated heat by the target walls (whose emissivity is high). There are two mechanisms for carrying such heat away: by convection to a heat sink or by vaporization of some liquid. The cup was designed so as to encourage convection as the primary mechanism for heat transfer (see Sec. II B and Fig. 2). By visual observation of the target with its radiation shield removed we made the, admittedly rather subjective, observation that the relative volume occupied by the bubbles could not possibly exceed 5%; that we doubt it could be over 2%; and we estimate it to be less than 1%.

From the observed rate of rise of bubbles and calculation of the heat absorbed by the target and feed lines we calculate that, if one-quarter of the heat ab-

sorbed is lost to bubbling, there will be at most 0.2% average density reduction in the interaction region.¹⁴ We rely on this result in applying a 0.2% correction to the data and assigning a $\pm 0.5\%$ uncertainty for this effect.

(v) Beam-Induced Bubbling

Ionization in the track of an electron results in local heating and the possibility of local boiling. We calculate, again assuming conservatively that as much as one-quarter of the heat lost by the beam develops into bubbles, that the effective density reduction is 0.3% with a 10^{-7} -A beam.

We have attempted to measure the effect by taking data at varying beam intensities. Figure 17 indicates the results. The picture is complicated by trigger dead-time effects discussed in Sec. IV D. The data are consistent with no effect and impose an upper limit of approximately 2% at 10^{-7} A.

We have used our calculation of 0.3% at 10^{-7} A to correct the data for beam-dependent bubbling—scaling the correction linearly with beam intensity. We assign errors equal to the correction. The greatest correction is a 0.4% correction at 100 F^{-2} . At 70 F^{-2} and below, the largest correction is 0.1%.

I. Energy of Incident Electrons

The cross section is a strongly varying function of the incident energy, being inversely proportional, for small energy variations, to between the fourth and seventh power of the energy (see Table I). It is necessary, therefore, to monitor the beam energy distribution very carefully.

Electrons were ejected at and on both sides of the peak of the accelerating cycle. We separately monitored the energy distribution of the beam relative to the peak energy and the value of the peak energy. The latter is a function of the field in the synchrotron magnets and, weakly, of the frequency of the accelerating rf field. We regularly monitored the necessary parameters during data runs so that the relative peak energy was known to better than $\pm 0.1\%$ at all times. The absolute energy calibration of the machine, relative to the monitoring parameters as used by us, was made by Winick.¹⁵ The uncertainty in that absolute energy calibration is $\pm 0.2\%$.

The electron synchrotron has an inherent energy spread of between ± 0.1 and $\pm 0.2\%$. The time spread of the ejected electrons results in a rather larger energy spread. The tail of the energy distribution can extend to 1 or 2% below the peak energy. The time distribution (from which the energy distribution can be directly deduced) was observed continuously on an oscilloscope screen. The magnetic field in the synchrotron

¹³ H. M. Roder, D. E. Diller, L. A. Weber, and R. D. Goodwin, *Cryogenics* **3**, 16 (1963).

¹⁴ See Sec. 4.8.d of Ref. 1 for details.

¹⁵ H. Winick, CEA Report No. CEA-1015 (unpublished).

at the time of occurrence of each computer trigger was also sampled and recorded by the computer. Although not an absolute measurement, this enabled the energy distribution to be determined relative to the peak energy. From these measurements the average energy was calculated. The correction to the energy was typically 0.2% and the error involved was typically $\pm 0.5\%$ in the cross section.

J. Angle of Scattering

The Rosenbluth formula has a basic $\sin^{-4}(\frac{1}{2}\theta)$ dependence. The $1/q^4$ dependence of the form factors introduces a further angular sensitivity. For the conditions of this experiment the cross-section dependence on angle ranged from θ^{-4} to θ^{-8} (see Table I). This strong angular dependence, typical of electromagnetic scattering, forces us to measure and monitor the scattered electron angle rather carefully.

Determination of the scattered angle is complicated by the extended size of the target and defining aperture and by the angular spread in the electron beam.

(i) Central Scattering Angle

The central angle was determined by knowing the relative positions of the target center, the center of the electron-defining aperture, and the beam position at a point downstream of the target. That position was chosen to be as near as possible opposite the defining aperture in order to reduce the sensitivity of the determination to the knowledge of where the beam passed through the target relative to the target center.

The beam position at the downstream point was monitored continuously using a tuned rf cavity mounted on a movable table. A glass slide was exposed to the beam occasionally to confirm the absolute beam position relative to fixed survey points.

The over-all error in the determination of the scattering angle, when the front aperture was employed, was in the region of $\pm 0.1\%$ with a consequent cross section uncertainty of about $\frac{1}{2}\%$. With the back aperture in use an additional error was introduced owing to a discrepancy in surveys and the uncertainty in scattering angle was then about $\pm 0.2\%$ at 20° .

Finally, a large but well-known correction had to be made to allow for the effect on both the incident and scattered electrons of the fringing fields of the proton arm-sweeping magnet. The resulting corrections to the cross sections, which are accurate to better than one-twentieth of their value, were approximately -2.5% at 20 , 30 , and 45 F^{-2} , -0.6% at 70 F^{-2} , and less than 0.1% at all other momentum transfers.

(ii) Finite Range of Angles

A range of angles is accepted due primarily to the finite acceptance of the spectrometer—but also to the finite length of the target and spread of directions of the incident beam. We have corrected the data for this

effect. The corrections amount to less than 1% and have an associated error of less than $\pm 0.1\%$.

K. Solid Angle

(i) Introduction

The acceptance of the system was defined by apertures in the electron spectrometer as described in Sec. II C (ii). The target-to-aperture distance was accurate to about $\pm 0.08 \text{ cm}$, which contributes an error about $\pm 0.1\%$ to the solid-angle determination and, hence, to the cross section.

(ii) Front Aperture

The front aperture was used in the 75-F^{-2} run and for all data at and below 30 F^{-2} . This aperture was located in front of the quadrupole magnet whose fringe field distorted the acceptance by less than 0.1% . Uncertainty in the aperture definition arises because electrons near the edge can be scattered back into the aperture before their energy has been sufficiently degraded. The aperture was designed to minimize such an uncertainty. Calculation suggests that the effective edge was within 0.0025 cm of the physical edge. We have used the aperture defined by the physical edge of the material and assign a 0.3% error, systematic to all measurements using the front aperture, due to this effect.

Surveying error is dominated by the target-position uncertainty. An additional $\pm 0.1\%$ uncertainty arises from possible skew of the aperture.

(iii) Rear Aperture

Edge uncertainties in the various components of the rear aperture [see Sec. II V (ii)] were negligible compared with surveying uncertainties in their positions, and notably in that of the stainless-steel vacuum tank. This led to an uncertainty of $\pm 0.5\%$ in the solid angle. A central obstacle limited trajectories near the horizontal plane of the system for both the upper and lower halves of the aperture simultaneously. There was an uncertainty of 0.25 cm in its vertical position. Such a displacement would affect the combined solid angle of both halves by much less than 0.1% but would affect the ratio of up-down to down-up trajectories by as much as 8% .

The principal uncertainty in the solid angle arises from the fact that, since the components of the aperture are in or behind the quadrupole, it is necessary to compute the solid angle on the basis of the known field. The error in computation and magnetic field measurement uncertainty would normally involve no more than a few tenths of a percent error. However, there is additional uncertainty due to certain aspects of the magnet performance which are not understood in terms of the measured field. We have estimated the

TABLE IX. Ratio of cross sections computed independently for down-up as compared with up-down trajectories. The errors are the statistical counting errors and do not include uncertainty in shower and Čerenkov counter efficiencies. An asterisk indicates that the rear aperture was used for the measurement.

q^2 (F^{-2})	$\frac{\sigma \text{ down-up}}{\sigma \text{ up-down}}$	q^2 (F^{-2})	$\frac{\sigma \text{ down-up}}{\sigma \text{ up-down}}$
7	0.998±0.014	70*	1.13±0.06
10	0.982±0.012	75	1.055±0.12
15	1.005±0.014	90*	1.003±0.034
20	1.008±0.02	100*	0.93±0.08
30	1.02±0.04	115*	0.90±0.08
45	1.05±0.08	130*	1.10±0.11
45*	0.998±0.03	150*	0.84±0.14

uncertainties which would arise from a number of types of field distortion or apparatus alignment. We feel that the error of $\pm 1\%$ which we place on the solid angle due to field-mapping uncertainties is a very conservative estimate.

(iv) Intercalibration of Apertures

The uncertainties in the magnetic field of the quadrupole and a wish to obtain a consistency check led us to take data in a high counting rate situation with both apertures. A fairly large electron angle (25.9°) was chosen so as to improve stability with respect to variations in the primary beam direction. The calculated ratio of the solid angles subtended by the two apertures was 0.451. The observed ratio was 0.452 (1 ± 0.015). The agreement is excellent and lends considerable confidence to our estimate of the solid angle subtended by the rear aperture.

(v) Ratio of Up-Down to Down-up Cross Sections

Although many errors cancel in comparing cross sections separately evaluated for the two trajectories, the performance of the counters themselves is checked by this means and gross errors in one trajectory would be revealed. Adding the two trajectories does, however, cancel certain errors in bin assignment and solid angle. We present, in Table IX, the ratio of the cross sections for the various runs. Data taken with the rear aperture are so indicated. The ratio of solid angles may differ from unity by $\pm 8\%$ for these runs due to misalignment of the components of the aperture. The comparison is considered very satisfactory.

L. Nominal Kinematics

We have chosen to define the elastic scattering kinematics of our data by the values of the incident electron energy and scattered electron angle. We make a small and precisely known correction to each cross section to be able to quote its value at nominal "round-figure"

values of the four-momentum transfer and either the incident electron energy or the scattered electron angle. The only error in such a correction comes from possible uncertainties in the change in form factors over the typical change of 1% in momentum transfer. From a comparison of the data with the dipole fit we estimate that, at worst, such a correction might be in error by $\pm 0.2\%$.

M. Radiative Corrections

(i) Meister and Yennie

Meister and Yennie¹⁶ have calculated the correction, $(1+\delta)^{-1}$, to be applied to an observed cross section in order to extract the theoretical cross section in the absence of radiation. Their δ is, in general, negative leading to observed cross sections which are smaller than the theoretical cross sections. They treat the case of an electron detected with good momentum resolution and very poor angular resolution and without coincident proton detection. They consider radiation by the proton as well as the electron lines.

Our basic radiative correction is that calculated by Meister and Yennie and written out in Eq. (4.1) of their paper.¹⁶ They state that the error is expected to be "of the order of 1% and probably not more than 2%." Since we have made some improvements (described below) to Meister and Yennie's calculation we have assigned to their calculation a $\pm 1\%$ error which is systematic to all our cross sections.

We have, as they proposed, exponentiated the doubly logarithmic terms in δ to include the contributions from unincluded higher-order terms in the perturbation-theory calculation.

An alternative calculation of the radiative correction is that of Tsai,¹⁷ who does the same physics as Meister and Yennie but makes some different calculational approximations. Mo and Tsai¹⁸ believe Tsai's approximations to be an improvement over those of Meister and Yennie. Use of the Tsai correction would result in our reporting cross sections slightly larger than our present estimate. The difference would be 0.3% at the lowest momentum transfer ($7 F^{-2}$) and 0.7% at the highest momentum transfer ($150 F^{-2}$).

(ii) Angular Restriction of Electrons

If a photon is radiated at a substantial angle to the direction of the scattered electron, the electron suffers an angular upset which results in a second-order correction to the cross section. However, the probability of sufficiently energetic photons being radiated at large angles is small and we estimate the effect on the cross section to be less than 0.1% and hence negligible.

¹⁶ N. Meister and D. Yennie, Phys. Rev. **130**, 1210 (1963).

¹⁷ R. Atkinson, III (private communication). Details are given in Sec. 4.13.d of Ref. 1.

¹⁸ L. Mo and Y. S. Tsai, Rev. Mod. Phys. **41**, 205 (1969).

(iii) Coincident Detection of Protons

The coincident proton detection places an angular constraint on the proton. An estimate of the radiative correction due to this effect has been made by Atkinson¹⁹ which leads to a correction of less than 0.2% in our experiment. The smallness of this correction is due to the deliberate oversize of the proton counters (see Sec. II D).

(iv) Variation of Matrix Element with Momentum Transfer

An assumption of Meister and Yennie's treatment is that the basic matrix element for the interaction of the electromagnetic field with the proton is not affected by the change in momentum transfer experienced by the exchanged photon when radiation takes place.

This assumption is not fully justified since quite appreciable changes in the matrix element (about 20% in its squared value) can accompany radiation of photons sufficiently hard to alter the scattered electron energy by, say, 3.5%. We hasten to add that *most* photons are soft and cause little upset. We have attempted to correct for this effect by estimating the variation in the matrix element when radiation occurs before scattering.²⁰ Form-factor variation with momentum transfer was included. This correction leads typically to a 1% change in cross section and we assign an error of one-quarter of the correction.

Mo and Tsai¹⁸ have recently published a review of radiative-correction calculations, primarily with regard to inelastic electron scattering, in which they include such an effect.

(v) Real Bremsstrahlung

The correction due to real bremsstrahlung is quite appreciable, being typically about 6%, but it can be precisely calculated. The form of the correction is contained in Bjorken's paper²¹ where the connection between radiative corrections and real bremsstrahlung is brought out clearly.

(vi) Width of Resolution Function

There is no additional correction to be made when the low-momentum cutoff in the acceptance is substantially below the elastic peak in units of, say, the FWHM of the momentum resolution function. However, if the cutoff is less than about 3 FWHM below the peak, the radiative correction is not quite that evaluated for the momentum interval between peak and cutoff. In this experiment the correction ranges from 0.1 to 0.5%. Details of the calculation are given in Ref. 1.

V. RESULTS**A. Evaluation of Cross Sections**

The cross sections were evaluated from the formula

$$d_0/d\Omega = \frac{(\text{number of scattered electrons}) \times (\text{correction factors})}{(\text{number of incident electrons}) \times N n \rho l \Delta\Omega},$$

where N is Avogadro's number, here taken to be 6.0225×10^{23} molecules/g molecule; n is the number of scatterers per molecule and is 2 for hydrogen; ρ is the density of target material in units of g molecule/cm³; l is the target length (in cm); $\Delta\Omega$ is the solid angle subtended by the detector in units of steradians.

The number of incident electrons is taken to be

$$\begin{aligned} & [\text{charge (Coulombs) collected by Faraday cup}] \\ & \quad \times 6.242 \times 10^{18}. \end{aligned}$$

The heart of the analysis lies in the various correction factors which we now discuss.

B. Discussion of Errors

We present a detailed breakdown of the analysis of some representative runs in Tables X and XI. Each table lists some 30 constituents of the cross-section calculation which are combined to provide a cross section and its related errors. Against each entry is a

reference to the section in this paper in which the correction is discussed.

Each constituent has associated with it a "value" and a multiplicative "correction factor." The value may be a component of the cross section or may be presented merely for interest. The correction factor is assumed to be unity if not specifically presented.

In estimating the errors associated with each constituent we have divided them into random and systematic errors. By systematic errors we mean to imply errors which are common to several measurements. However, there are complications. The absolute calibration of the synchrotron energy is, for example, subject to a $\pm 0.2\%$ systematic error—a future measurement may improve and change our estimate of that quantity. However, the effect of this uncertainty on the cross sections varies from ± 0.8 to $\pm 1.4\%$ depending on the energy dependence of the cross section (see Table I). Thus, some "systematic" errors are not the same for all cross sections. Then, too, cross sections measured with the back aperture have a common 1.2%

¹⁹ Details are given in Sec. 4.13.e of Ref. 1.

²⁰ See Sec. 4.13.e of Ref. 1 for details.

²¹ J. D. Bjorken, *Ann. Phys. (N.Y.)* **24**, 201 (1963).

TABLE X. Constituents of the cross sections at 7, 45, and 70 F⁻².

	7 F ⁻² ; 20°				45 F ⁻² ; 20°				70 F ⁻² ; 5.5 GeV							
	Subsection in Sec. IV	Value	Cor- rection		Fractional error		Value	Cor- rection		Fractional error		Value	Cor- rection		Fractional error	
			factor	factor	System- atic	Random		factor	factor	System- atic	Random		factor	factor	System- atic	Random
Number of accepted events (both trajectories)	B	20159	1.001	0.007	0.001	0.001	3874	1.0075	0.016	0.0075	0.001	996	1.004	0.032	0.004	0.004
Uncertainty in event selection	B(i)(ii)		1.000					1.000					1.000			
Events lost in tails of momentum resolution	B(iii)		1.01		0.01			1.009		0.008			1.0085		0.0085	
Computer trigger efficiency	D(i)		1.014					1.005					1.0034			
Computer dead-time	D(ii)		1.048					1.010	0.002				1.046	0.015		
Proton counter efficiency	E		0.999	0.001				0.999	0.001				0.998	0.002		
Correction from accidental proton coincidences	E		1.013	0.003				1.0015	0.001				1.056	0.015		
Shower counter efficiency	F		1.000					1.012					1.084	0.005		
Cerenkov counter efficiency	F		1.132		0.01			1.150		0.01			1.165		0.01	
Radiative correction (Meister & Yennie)	M(i)		0.994		0.002			0.988		0.003			0.998		0.003	
Correction due to variation of matrix element with q^2	M(iv)															
Correction due to width of momentum resolution	M(vi)		1.002					1.002					1.002			
Correction due to real bremsstrahlung	M(v)		1.054	0.005				1.044	0.005				1.055	0.005		
Empty target subtraction	C(i)		0.994	0.002				0.990	0.002				0.991	0.002		
Contamination from inelastic electroproduction	C(iv)		1.000					0.980	0.01				0.958	0.02		
Pion contamination and electrons from Dalitz decay	C(iii)		1.000	0.002				1.000	0.002				1.000	0.002		
Uncertainty because above-peak is nonzero	C(ii)		1.000	0.001				1.000	0.005				1.000	0.003		
Faraday cup charge (units of 10 ⁻⁴ C)	G(i)		0.3007				2.962	1.000		0.0025		4.429	1.000		0.0025	
Faraday cup efficiency	G(i)		1.000		0.0025			1.000					1.000			
Integrator calibration	G(iii)		0.998	0.001				1.001	0.001				0.997	0.001		
Faraday cup/S.E.M. ratio	G(ii)		2.71				2.42					2.26				
Target length (inches of cold hydrogen)	H(i)(ii)		2.173	0.0025			2.153	0.0025				2.173	0.0025			
Target density (g moles/cm ³)	H(iii)		0.0351	0.0015			0.0351	0.0015				0.0351	0.0015			
Correction due to bubbling of hydrogen	H(iv)(v)		1.005	0.005	0.005			1.005		0.005			1.005		0.005	
Synchrotron peak energy (GeV)	I		1.569		0.008		4.327	1.005		0.013		5.535	1.005		0.014	
Energy averaged over spill (GeV)	I		1.566	0.004			4.321	0.004				5.526	0.004			
Average electron scattering angle (deg)	J(i)		20.07	0.005			19.85	0.008				20.13	0.008			
Solid angle (msr)	K		0.829		0.003		1.814	0.003		0.012		1.824	0.003		0.012	
Correction due to extended angular acceptance	J(ii)		0.999				0.994	0.994				0.993	0.993			
Correction to bring to nominal kinematics	L		0.989	0.002			0.962	0.962				1.0233	1.0233		0.002	
Total correction			1.3824				1.1591	1.1591				1.4279	1.4279			
Fractional errors added in quadrature			0.0122	0.0176			0.0229	0.0229				0.046	0.046			
Fractional errors added directly			0.0380	0.0415			0.0660	0.0660				0.124	0.124			

TABLE XI. Constituents of the cross sections at 100, 130, and 150 F⁻².

	Subsection in Sec. IV	100 F ⁻² ; 5.5 GeV			130 F ⁻² ; 6 GeV			150 F ⁻² ; 6 GeV		
		Value	Cor- rection factor	Fractional error System- atic Random	Value	Cor- rection factor	Fractional error System- atic Random	Value	Cor- rection factor	Fractional error System- atic Random
Number of accepted events (both trajectories)	B	601		0.041	333		0.055	239		0.065
Uncertainty in event selection	B(i) (ii)		1.005	0.005		1.0125	0.0125		0.9547	0.05 0.005
Events lost in tails of momentum resolution	B(iii)		1.000			1.002	0.001		1.0025	0.001
Computer trigger efficiency	D(i)		1.0176	0.0125		1.0176	0.0125		1.015	0.010
Computer dead-time	D(ii)		1.007			1.016			1.008	
Proton counter efficiency	E		1.026	0.01		1.026	0.01		1.026	0.010
Correction from accidental proton coincidences	E		0.998	0.001		0.998	0.001		0.998	0.001
Show counter efficiency	F		1.010	0.005		1.015	0.008		1.018	0.002
Čerenkov counter efficiency	F		1.079	0.007		1.046	0.008		1.000	
Radiative correction (Meister and Yennie)	M(i)		1.163	0.01		1.176	0.01		1.189	0.030 0.01
Correction due to variation of matrix element with q^2	M(iv)		0.9845	0.003		0.987	0.003		0.988	0.003
Correction due to width of momentum resolution	M(vi)		1.0035			1.003			1.005	
Correction due to real bremsstrahlung	M(v)		1.070	0.005		1.067	0.005		1.075	0.005
Empty target subtraction	C(i)		0.994	0.002		0.993	0.002		0.994	0.002
Contamination from inelastic electroproduction	C(iv)		0.985	0.008		0.964	0.018		0.967	0.016
Pion contamination and electrons from Dalitz decay	C(iii)		1.000	0.002		1.000	0.002		1.000	0.002
Uncertainty because above-peak is nonzero	C(ii)		1.000	0.002		0.994	0.006		0.985	0.015
Faraday cup charge (units of 10 ⁻⁴ C)	G(i)	13.85			40.96			64.10		
Faraday cup efficiency	G(i)		1.000	0.0025		1.000	0.0025		1.000	0.0025
Integrator calibration	G(iii)		1.000	0.001		1.000	0.001		1.000	0.001
Faraday cup/S.E.M. ratio	G(ii)	2.30			2.34			2.33		
Target length (inches of cold hydrogen)	H(i) (ii)	3.545		0.009	2.966		0.002	3.545		0.009
Target density (g mols/cm ³)	H(iii)	0.0351		0.0015	0.0351		0.0015	0.0351		0.0015
Correction due to bubbling of hydrogen	H(iv) (v)		1.009	0.009		1.0085	0.0075		1.0065	0.0065
Synchrotron peak energy (GeV)	I	5.527		0.014	6.031		0.014	6.031		0.014
Energy averaged over spill (GeV)	I	5.511		0.005	6.011		0.007	6.007		0.007
Average electron scattering angle (deg)	J(i)	26.13		0.018	29.14		0.015	33.60		0.015
Solid angle (msr)	K	1.822		0.012	1.819		0.001 0.012	1.820		0.012
Correction due to extended angular acceptance	J(ii)		0.996			0.997			0.998	
Correction to bring to nominal kinematics	L		0.968	0.002		0.9775	0.002		0.976	
Total correction			1.3461			1.3246			1.2019	
Fractional errors added in quadrature				0.049 0.027			0.063 0.029			0.093 0.025
Fractional errors added directly				0.120 0.068			0.146 0.074			0.235 0.063

TABLE XII. Final cross sections.

Kinematics		Counting statistics	Fractional errors		Cross section units of 10^{-32} Cm ² /sr	Total fractional error in cross section	Ratio of cross section to dipole fit prediction
Four-momentum transfer (F^{-2})	Incident energy or scattered angle		Other random errors	Systematic errors			
7.00	20.00 deg	0.007	0.010	0.018	76.75	(1±0.021)	0.915
10.00	20.00 deg	0.006	0.012	0.018	41.19	(1±0.022)	1.009
15.00	20.00 deg	0.007	0.018	0.018	15.64	(1±0.026)	0.981
20.00	20.00 deg	0.010	0.012	0.016	7.595	(1±0.023)	1.017
30.00	20.00 deg	0.032	0.025	0.020	2.398	(1±0.045)	1.076
30.00	20.00 deg	0.020	0.011	0.019	2.304	(1±0.029)	1.035
45.00	20.00 deg	0.039	0.017	0.019	0.6056	(1±0.046)	1.075
45.00	20.00 deg	0.016	0.016	0.024	0.5792	(1±0.033)	1.028
70.00	5.500 GeV	0.032	0.033	0.024	0.1209	(1±0.052)	1.173
75.00	6.000 GeV	0.060	0.051	0.022	0.0958	(1±0.081)	1.068
90.00	6.000 GeV	0.018	0.033	0.026	0.0364	(1±0.046)	1.195
100.0	5.500 GeV	0.041	0.027	0.027	0.0135	(1±0.056)	1.144
115.0	6.000 GeV	0.038	0.032	0.027	0.00725	(1±0.056)	1.139
130.0	6.000 GeV	0.055	0.030	0.029	0.00298	(1±0.069)	1.095
150.0	6.000 GeV	0.065	0.066	0.025	0.00104	(1±0.096)	1.104

systematic error which is not shared with measurements made using the front aperture. We have, nevertheless, included this as a systematic error on the basis that it is more systematic than random.

Another class of errors which has given us pause for thought is that associated with measurements whose errors are asymmetric. The bubbling correction to the hydrogen density is an example. It can only reduce the density so that, in the sense in which we apply them, its correction factor must be greater than or equal to unity. We believe that the correction is most probably small but can not completely rule out an effect considerably larger than our (small) "most-probable" estimate. Rather than attempt to construct an asymmetric likelihood function, which is a more elaborate procedure than our understanding of these effects warrants, we have estimated the maximum possible correction and applied one-half of it while incorporating a symmetric error equal to the applied correction.

The random errors quoted are estimates of the change in cross section from a 1 *standard deviation* in the measurement. We do not, in general, include errors less than ±0.2%.

For each table we evaluate the product of all correction factors (total correction) and the total random and systematic errors added both in quadrature and directly. The straight sum of the errors is presented for

interest and as an absolutely outside limit on the error. The addition in quadrature is our best estimate of the errors. To assign an over-all error we have taken the sum, in quadrature, of the random and systematic errors. This procedure is reasonable but not necessarily correct and our results must be considered with an eye to the systematic errors.

The dominant errors in the cross sections are the following:

(1) Statistical fluctuations in the number of accepted events, which dominate the high-momentum-transfer data (above about 70 F^{-2}).

(2) Uncertainties in event selection, due mainly to the problem of assigning code-77 events as discussed in Sec. IV E (i). At momentum transfers above about 45 F^{-2} this effect gave rise to an uncertainty of as much as ±1%.

(3) The computer trigger was intended to be 100% efficient, but unforeseen dead-time effects gave rise to corrections of as much as 1 to 2% with uncertainties of the same magnitude.

(4) The radiative corrections were rather carefully computed with several effects not generally considered in previous scattering experiments having been made (see Sec. IV M). We assign a ±1.0% systematic error to our correction based on the uncertainty estimated by Meister and Yennie.¹⁶

TABLE XIII. Cross sections of Ref. 22. The cross sections are for the stated incident energy and scattered angle. The momentum transfers are provided for convenience.

Kinematics				Fractional errors			Cross section units of 10^{-32} cm ² /sr	Total fractional error in cross section	Ratio of cross section to dipole fit prediction
Four-momentum transfer squared (F^{-2})	Scattered electron angle (degrees)	Incident electron energy (GeV)	Counting statistics	Other random errors	Systematic errors				
1.413	0.055	6.77	0.0081	0.046	0.016	8720	0.049	1.017	
3.724	0.145	6.76	0.012	0.030	0.016	2270	0.036	0.965	
6.858	0.267	6.67	0.012	0.030	0.016	830.0	0.036	0.938	
10.839	0.442	8.64	0.0087	0.030	0.016	189.0	0.035	1.003	
16.694	0.650	9.55	0.0093	0.030	0.016	64.20	0.035	1.051	

(5) Contamination from inelastic electroproduction has been carefully computed using the theory of Adler.⁸ Nevertheless, at momentum transfers above about $45 F^{-2}$ there are uncertainties in the subtraction of from ± 1 to $\pm 2\%$.

(6) Uncertainties in target length have led to errors of from ± 0.3 to $\pm 1\%$.

(7) Uncertainty in the absolute energy calibration

of the accelerator ($\pm 0.2\%$) leads to systematic uncertainties in the cross sections of from ± 0.8 to $\pm 1.4\%$.

(8) The uncertainty in the measurement of the electron-scattering angle leads to errors of from $\pm \frac{1}{2}$ to $\pm 1\frac{1}{2}\%$.

(9) The solid angle of the electron spectrometer was uncertain to $\pm 0.3\%$ (front aperture) or $\pm 1.2\%$ (rear aperture).

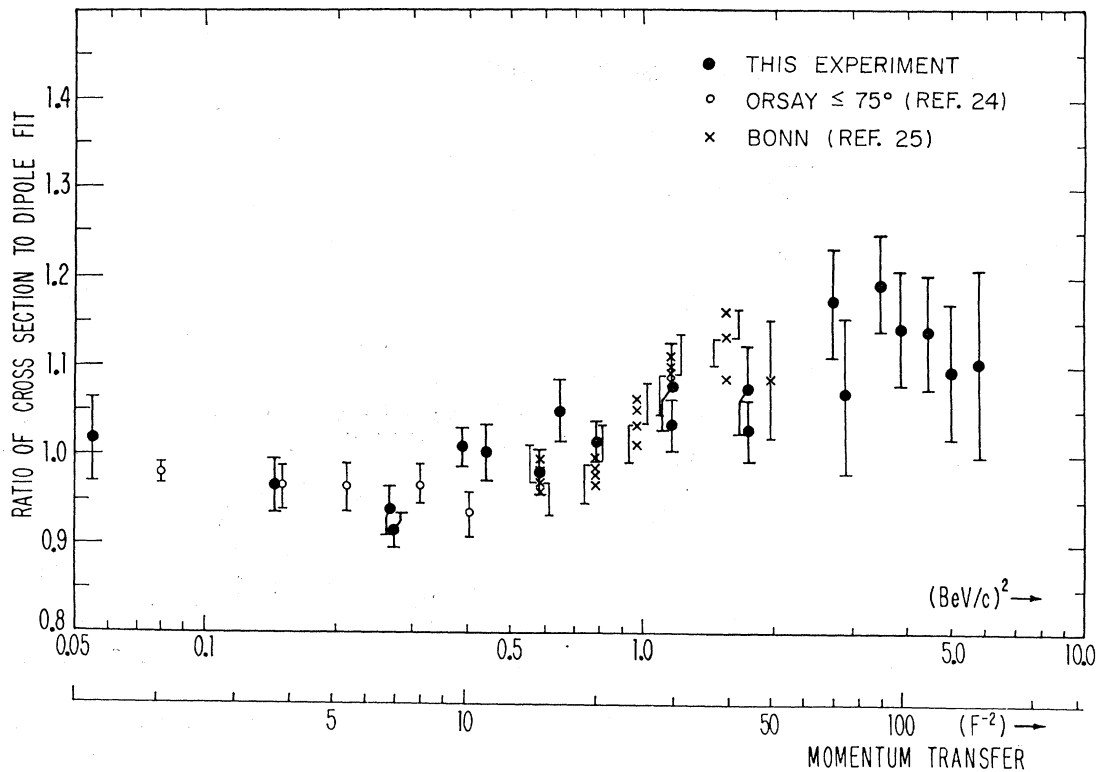


Fig. 18. Comparison of the data from the present experiment with data of Refs. 24 and 25. Data from all laboratories are plotted as ratios to the "dipole"-fit prediction with a constant of 0.71 (GeV/c)².

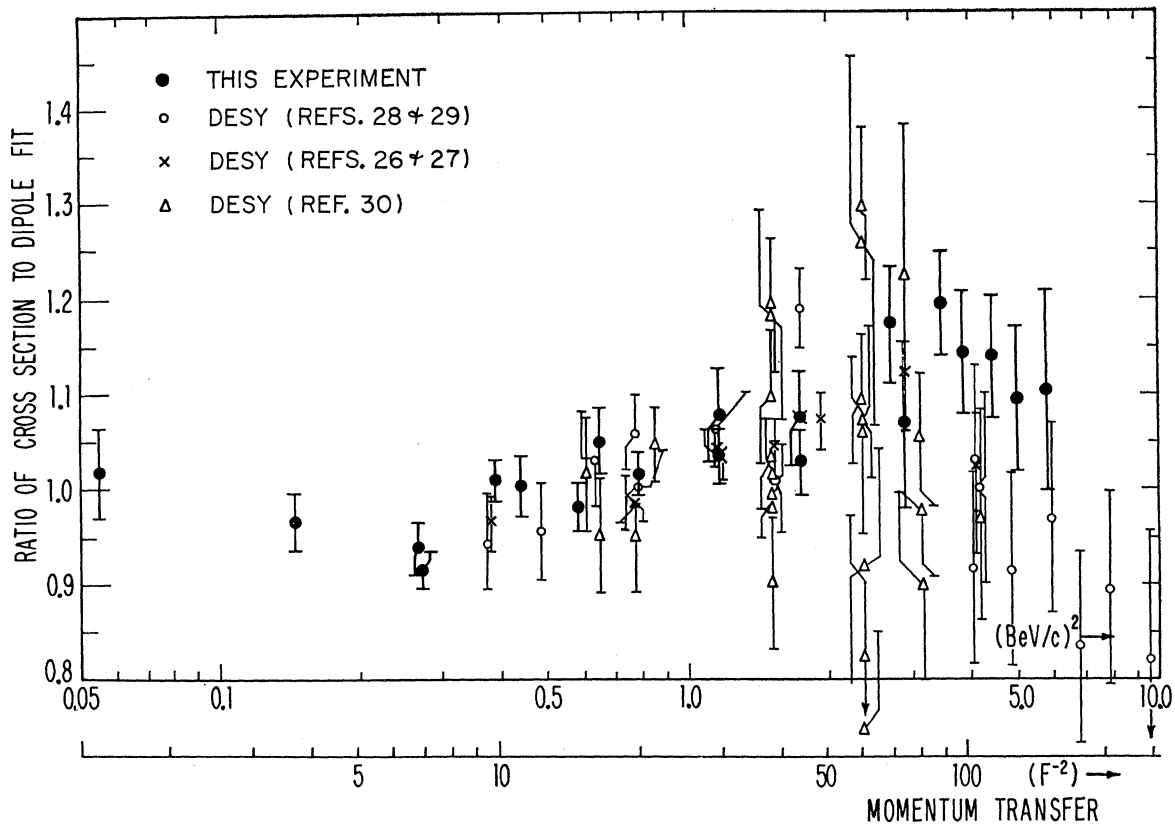


FIG. 19. Comparison of the data from the present experiment with the data of Refs. 26-30.

The contributions from other sources of error can be ascertained from Tables X and XI and are generally smaller than the above effects. The reader is referred to the relevant sections of this article specified in the tables for a discussion of the individual effects.

The final cross sections are presented in Table XII. We list separately the counting statistical fluctuations, contributions from other sources of random error, and systematic errors. Our final over-all error (standard deviation) is obtained by adding these in quadrature.

We also give, in Table XIII, the elastic electron-proton scattering cross sections determined by Mistretta *et al.*²² Their experiment was performed on the same apparatus as the present experiment and they were led to measure elastic electron-proton cross sections as normalization points. They used essentially the same analysis procedure as in the present experiment, but proceeded independently of the present analysis.

A preliminary analysis of this experiment was reported in Ref. 3. While correct to within the stated errors the previous analysis is to be regarded as superseded by the present data which are the results of a

more complete analysis and contain some new unpublished results.

The present experiment represents an improvement over previous forward-angle measurements made in this laboratory⁵ and should be regarded as superseding them.

C. Comparison with Other Data

In comparing our data with data from other laboratories we make use of a technique first introduced in Ref. 3 in which the measured cross sections are divided by a calculated cross section which is evaluated using the Rosenbluth formula²³ in conjunction with some model for the form factors. In this way almost all the momentum-transfer dependence is cancelled out of the cross section and one is left with a ratio which differs from unity due either to deficiencies in the model for the form factors or to errors in the measured cross sections or to both. Provided the deficiencies in the form-factor model vary fairly slowly with both momentum transfer and, say, angle this provides a powerful technique for interpolating and comparing data.

²² C. Mistretta, J. A. Appel, R. J. Budnitz, L. Carroll, J. Chen, J. R. Dunning, Jr., M. Goitein, K. Hanson, D. Imrie, and Richard Wilson, *Phys. Rev.* **184**, 1487 (1969).

²³ See, for example, L. N. Hand, D. G. Miller, and Richard Wilson, *Rev. Mod. Phys.* **35**, 335 (1963), where the form factors we use are also written out.

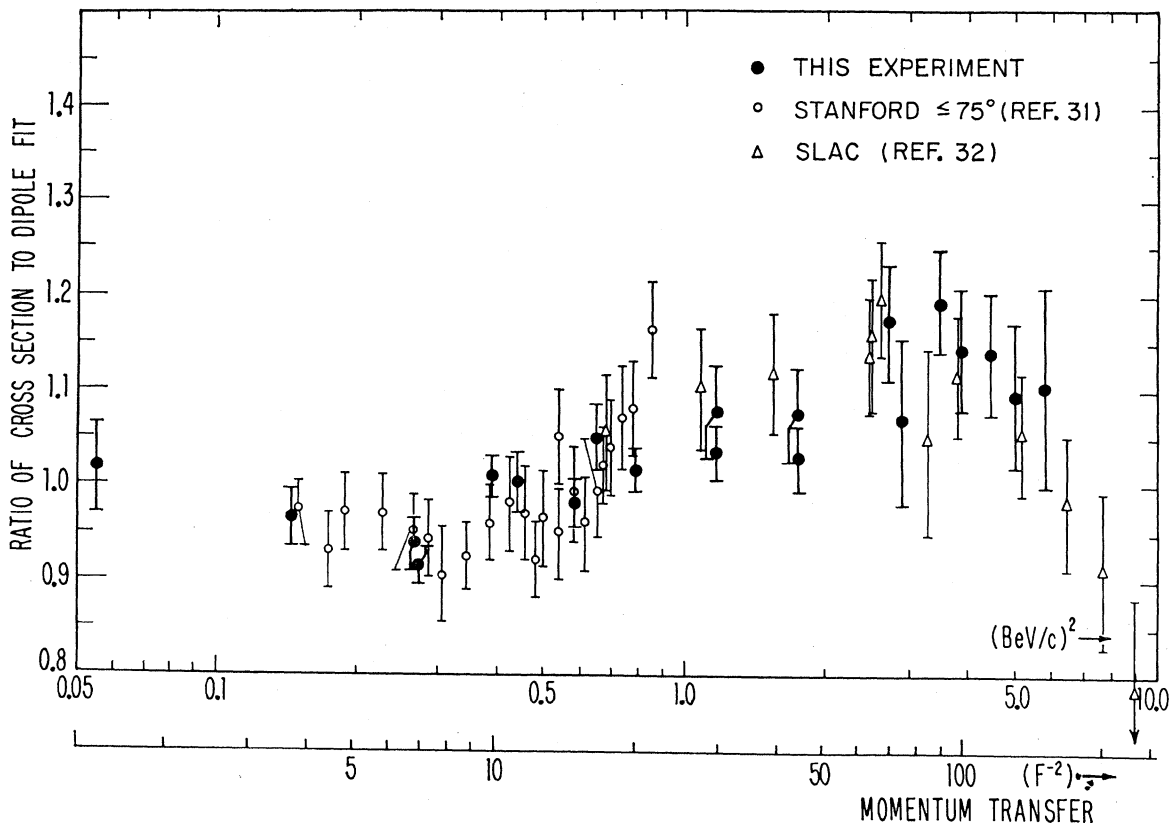


Fig. 20. Comparison of the data from the present experiment with the data of Refs. 31 and 32. The data of Ref. 32 have the quoted systematic error of 6% folded in quadrature with the statistical errors to conform with common usage.

The model we pick for the form factors is the so-called dipole fit [with a constant of 0.71 (GeV/c)^2] combined with the scaling law

$$G_{ep}(q^2) = G_{mp}(q^2)/\mu_p = [1 + q^2/0.71 \text{ (GeV/c)}^2]^{-2}.$$

This model does indeed fit the data over all regions of momentum transfer and angle presently measured to within about $\pm 15\%$. The approximate validity of the scaling law combined with the great insensitivity of high-momentum-transfer data to G_{ep} imply, then, that this technique for comparing data is probably accurate to the order of 1 or 2%.

With the plethora of data now in existence one cannot display the data of all laboratories on one comprehensible graph. We have, therefore, divided the data into three separate groups with no motive other than clarity of presentation in mind. Thus, we present in Fig. 18 a comparison of the present data with that of Lehmann *et al.*²⁴ and Berger *et al.*²⁵ We observe agree-

ment within the errors with these groups with the possible exception of the Berger data²⁵ above 1 (GeV/c)^2 where their data appear to be a few percent higher than ours. Their data are taken at fairly backward angles and this apparent discrepancy is just the manifestation of their observation of the ratio $\mu G_e/G_m$ being less than unity at their higher momentum transfers.

In Fig. 19 we compare our data with those of Bartel *et al.*,^{26,27} Albrecht *et al.*,^{28,29} and Behrend *et al.*³⁰ We observe excellent agreement to within the stated errors with all groups with the exception that above about 3 (GeV/c)^2 our data are consistently higher by some 10 to 15% than those of these groups. Also, above 1 (GeV/c)^2 , the data of Albrecht *et al.* show a spread rather outside of the errors.

²⁶ W. Bartel, B. Dudelzak, H. Krehbiel, J. M. McElroy, U. Meyer-Berkhout, R. J. Morrison, H. Nguyen Ngoc, W. Schmidt, and G. Weber, Phys. Rev. Letters **17**, 608 (1966).

²⁷ W. Bartel, B. Dudelzak, H. Krehbiel, J. M. McElroy, U. Meyer-Berkhout, R. J. Morrison, H. Nguyen Ngoc, W. Schmidt, and G. Weber, Phys. Letters **25B**, 236 (1967).

²⁸ W. Albrecht, H. J. Behrend, F. W. Brasse, W. Flauger, H. Hultschig, and K. G. Steffen, Phys. Rev. Letters **17**, 1192 (1966).

²⁹ W. Albrecht, H. J. Behrend, H. Dörner, W. Flauger, and H. Hultschig, Phys. Rev. Letters **18**, 1014 (1967).

³⁰ H. J. Behrend, F. W. Brasse, J. Engler, H. Hultschig, S. Galster, G. Hartwig, H. Schopper, and E. Ganssauge, Nuovo Cimento **48**, 140 (1967).

²⁴ P. Lehmann, R. Taylor, and Richard Wilson, Phys. Rev. **126**, 1183 (1962); B. Dudelzak, G. Sauvage, and P. Lehmann, Nuovo Cimento **28**, 18 (1963); P. Lehmann, in *Proceedings of the Twelfth International Conference on High Energy Physics, Dubna, 1964* (Atomizdat, Moscow, 1965).

²⁵ Chr. Berger, E. Gersing, G. Knop, B. Langenbeck, K. Rith, and F. Schumacher, Phys. Letters **28B**, 276 (1968).

In Fig. 20 we compare our data with the more forward angle data ($\leq 75^\circ$) of Janssens *et al.*³¹ and the recent data of Coward *et al.*³² There is excellent agreement with Janssens *et al.* up to about $0.65 \text{ (GeV}/c)^2$ above which our data lie some 5% below theirs. The data of Coward *et al.* are some 5% higher than our data below $2 \text{ (GeV}/c)^2$ and are in good agreement with our data above that momentum transfer.

Thus we see that the data from several laboratories are fairly consistent. There are, in some instances, discrepancies of as much as 10% which remain to be resolved. We wish to emphasize that the data are clearly and unequivocally not fit *in detail* by the dipole fit. The discrepancy is not to be found in experimental error—nor can it be remedied by other choices of the free parameter in the model. Nevertheless, the fit is a remarkably good representation of the gross momentum transfer dependence of the form factors to within about $\pm 15\%$ in the value of the square of the form factors.

³¹ T. Janssens, R. Hofstadter, E. B. Hughes, and M. R. Yearian, *Phys. Rev.* **142**, 922 (1966).

³² D. H. Coward, H. DeStaebler, R. A. Early, J. Litt, A. Minten, L. W. Mo, W. K. H. Panofsky, R. E. Taylor, M. Breidenbach, J. I. Friedman, H. W. Kendall, P. N. Kirk, B. C. Barish, J. Mar, and J. Pine, *Phys. Rev. Letters* **20**, 292 (1968). In the figures of this paper we have combined these authors' statistical error with their quoted 6% systematic error to conform to common usage.

VI. CONCLUSIONS

We have reported measurements of elastic electron-proton data taken in the range of four-momentum transfers of from 7 F^{-2} [$0.27 \text{ (GeV}/c)^2$] to 150 F^{-2} [$5.84 \text{ (GeV}/c)^2$] and at electron scattering angles in the range of 20° to 34° . The accuracy of the low-momentum-transfer data, which are dominated by systematic errors, is estimated at $\pm 2.1\%$. The feature of this experiment which gives us considerable confidence in the results is our ability to remove a redundant kinematic constraint on the process, namely, the requirement of a proton coincidence, with no appreciable change in computed cross section (see Table VIII).

ACKNOWLEDGMENTS

We wish to acknowledge our considerable debt to the Harvard Cyclotron shops headed by M. Wanagel, J. McElaney, R. Wharton, and W. Dunn and to the Cambridge Electron Accelerator staff under the direction of M. Stanley Livingston. In particular, the assistance of J. Cerino, F. Dell, M. Fotino, J. M. Paterson, G. Voss, and H. Winick is gratefully acknowledged. Finally, we were greatly helped by Professor N. Ramsey and Professor J. K. Walker in the initial stages of the experiment.